# Diadenosine tetraphosphate regulates biosynthesis of GTP in Bacillus subtilis

Pietro I. Giammarinaro[1,4], Megan K. M. Young[2,4], Wieland Steinchen[1], Christopher-Nils Mais[1], Georg Hochberg[1,3], Jin Yang[2], David M. Stevenson[2], Daniel Amador-Noguez[2], Anja Paulus[1], Jue D. Wang[2,*], Gert Bange[1,3*]

**Affiliations**

[1]Philipps University Marburg, Center for Synthetic Microbiology & Department of Chemistry, Marburg, Germany.
[2]University of Wisconsin-Madison, Department of Bacteriology, Madison, USA.
[3]Max Planck Institute for Terrestrial Microbiology, Marburg, Germany.
[4]These authors contributed equally.

*Correspondence:
wang@bact.wisc.edu
gert.bange@synmikro.uni-marburg.de

Diadenosine tetraphosphate (Ap4A) is a putative second messenger molecule that is conserved from bacteria to man. Nevertheless, its physiological role, and the underlying molecular mechanisms, are poorly characterized. We investigated the molecular mechanism by which Ap4A regulates inosine-5'-monophosphate dehydrogenase (IMPDH, a key branching point enzyme for the biosynthesis of adenosine or guanosine nucleotides) in *Bacillus subtilis*. We solved the crystal structure of *Bs*IMPDH bound to Ap4A at a resolution of 2.45 Å to show that Ap4A binds to the interface between two IMPDH subunits, acting as the glue that switches active IMPDH tetramers into less active octamers. Guided by these insights, we engineered mutant strains of *B. subtilis* that bypass Ap4A-dependent IMPDH regulation without perturbing intracellular Ap4A pools themselves. We used metabolomics suggesting that these mutants have a dysregulated purine, and in particular GTP, metabolome and phenotypic analysis showing increased sensitivity of *B. subtilis* IMPDH mutant strains to heat compared with wild-type. Our study identifies a central role for IMPDH in remodelling metabolism and heat resistance, and provides evidence that Ap4A can function as an alarmone.

# MAIN

# INTRODUCTION

Nucleotide-based second messengers, e.g., (p)ppGpp[1,2], c-di-GMP,[3,4] or c-di-AMP[5], are essential for bacterial responses to changing environmental and stress conditions. Diadenosine polyphosphate molecules such as diadenosine 5',5'''-P1,P4-tetraphosphate (Ap4A) have been known since the 1960's[6] and are found in all domains of life[7]. Ongoing debate is whether they are damage metabolites[8] or *bona fide* second messengers[7].

Ap4A is comprised of two adenosines bridged at their 5' ends by four phosphates (**Fig. 1a**). It is primarily produced by aminoacyl-tRNA synthetases, with lysyl-tRNA synthetase (LysRS) being a prominent example, under heat shock and oxidative stress conditions through the transfer of the aminoacylated AMP onto the 5' γ-phosphate of ATP [6,9–11]. The promiscuous utilization of other aminoacyl-AMP acceptors by LysRS, such as ADP, GDP or GTP leading to the synthesis of the even more enigmatic Ap3A, Ap3G and Ap4G, respectively, broadens the spectrum of dinucleoside polyphosphate molecules[10].

Several studies have reported pleiotropic roles for Ap4A in bacteria. In *Escherichia coli* Ap4A has been implicated in cell division[12], motility[13] and responses to heat/oxidative stress[14] and aminoglycoside antibiotics[15]. Ap4A has been associated with sporulation in *Myxococcus xanthus*[16], heat shock, ethanol stress, and cell oxidation in *Salmonella typhimurium*[10], biofilm formation in P*seudomonas aeruginosa*[17], and survival of *Helicobacter pylori* in response to oxidative stress[18].

Our knowledge about Ap4A-binding partners in bacteria and a mere understanding of the mechanisms by which Ap4A regulates these is currently limited to *E. coli*[8,14,19,20]. Proposed targets include the chaperones DnaK, ClpB and GroEL[14,21] and the *de novo* purine nucleotide biosynthesis enzyme inosine-5'-monophosphate dehydrogenase (IMPDH)[8,19]. These screens employed biotin and/or aziridine-modified Ap4A to enrich Ap4A-binding proteins, which potentially may have biased the target spectrum due to the size of the modifier groups.

# RESULTS

### Identification of Ap4A targets in *Bacillus anthracis*.

To identify further Ap4A targets in unbiased manner, we used a radioactively-labelled but otherwise chemically unmodified Ap4A as bait in a differential radial capillary action of ligand assay (DRaCALA) assay[22]. Simultaneously, we aimed to expand knowledge on Ap4A regulation to the Firmicutes phylum. Having a library for all *Bacillus anthracis* proteins available, we screened for Ap4A-binding targets in this organism and then continued our mechanistic and physiological analyses in *Bacillus subtilis*. We employed two *B. anthracis* overexpression libraries, each including 5,341 open reading frames (ORFs) N-terminally fused to either hexa-histidine (His) or His-maltose binding protein (His-MBP)[23]. Both libraries were overexpressed in *E. coli*, and the binding of radio-labelled [$^{32}$P]-Ap4A to the lysates assayed by DRaCALA[22]. This screen identified inosine-5'-monophosphate dehydrogenase (IMPDH, gene: *guaB*) as putative Ap4A-binding partner (**Fig. 1b**).

IMPDH catalyzes the nicotinamide adenine dinucleotide ($NAD^+$)-dependent conversion of inosine-5'-monophosphate (IMP) into xanthosine-5'-monophosphate (XMP)[24]. XMP represents the start for the generation of GMP, GDP, and GTP. Moreover, IMPDH represents the branching point in the biosynthesis of adenosine and guanosine nucleotides (**Fig. 1c**).

To further probe the Ap4A-IMPDH interaction, we investigated IMPDH from *B. subtilis* (*Bs*), because this bacterium is broadly studied and a close relative of *B. anthracis*. Isothermal titration calorimetry (ITC) revealed a dissociation constant ($K_d$) of 7.4 ± 2.1 μM for the Ap4A-*Bs*IMPDH interaction (**Fig. 1d, Extended Data Fig. 1e**). This $K_d$ is within the range of Ap4A concentration determined by LC-MS for exponentially growing *B. subtilis* (**Fig. 1d**). We also tested the binding of the adenosine nucleotides AMP, ADP, and ATP to *Bs*IMPDH due to their structural similarity to Ap4A and because an ATP-dependent stimulation of IMPDH activity in

*P. aeruginosa* (*Pa*) was reported[25]. Binding of AMP and ATP to *Bs*IMPDH proceeds with low affinity evidenced by $K_d$ values of approximately 18 and 5 mM, respectively. No interaction was found for ADP (**Fig. 1d, Extended Data Figs. 1a-c**). Furthermore, we tested the specificity of *Bs*IMPDH for the nucleobases linked by the phosphates in the dinucleotides and the length of this phosphate linker by probing the binding of Ap*n*A and Ap*n*G compounds. Ap*n*A dinucleotides Ap3A, Ap5A, and Ap6A bound to *Bs*IMPDH with $K_d$'s of 62.0 ± 10.9 μM, 30.4 ± 23.5 μM and 0.8 ± 0.2 μM, respectively (**Fig. 1d, Extended Data Figs. 1d**, **f**, **g**). No binding was found for the Ap*n*G dinucleotides Ap3G, Ap4G, and Ap5G (**Fig. 1d, Extended Data Figs. 1h-j**). Collectively, *Bs*IMPDH had a strong preference (≥100-fold higher affinity) for Ap*n*A dinucleotides with varying phosphor-linker lengths over the related adenosine mononucleotides.

**Ap4A is a non-competitive inhibitor of IMPDH.**

Next, we probed whether Ap4A and Ap*n*A would affect IMPDH activity by an assay based on the reduction of the $NAD^+$ cofactor to NADH detectable at a wavelength of 340 nm. At constant saturating $NAD^+$ and variable IMP concentrations without Ap4A supplemented, *Bs*IMPDH showed a Michaelis-Menten-like kinetic behavior, with maximal velocity ($V_{max}$) and Michaelis-Menten constant ($K_m$) values of 6.3 μM $min^{-1}$ and 63 μM, respectively (**Fig. 1e, Extended Data Fig. 2a**). With increasing Ap4A concentration, $V_{max}$ decreased while $K_m$ remained unaltered, suggesting an allosteric mode of inhibition. *Bs*IMPDH inhibition by Ap4A proceeded with an inhibitory constant ($K_i$) of 15.8 μM roughly reflecting the $K_d$ between Ap4A and *Bs*IMPDH (**Fig. 1e, Extended Data Fig. 2a**). At constant saturating IMP and variable $NAD^+$ concentrations *Bs*IMPDH activity showed a similar decline of $V_{max}$ dependent on increasing Ap4A concentrations (**Fig. 1e, Extended Data Fig. 2b**). In contrast to Ap4A, which potently reduced *Bs*IMPDH activity, adenosine mononucleotides only moderately inhibited *Bs*IMPDH (**Fig. 1f, Extended Data Fig. 2a**). Ap*n*G dinucleotides did not alleviate *Bs*IMPDH activity and out of the Ap*n*A dinucleotides tested by us, only Ap5A and Ap6A resulted in *Bs*IMPDH inhibition (**Figs. 1g**, **h, Extended Data Fig. 2a**). Despite Ap5A and Ap6A being the most potent inhibitors of *Bs*IMPDH, we focused our further studies on Ap4A because it was more abundant than other dinucleotides in *B. subtilis in vivo* (**Fig. 1d**). Likewise, Ap4A was approximately 3-fold more abundant than Ap5A under various stress conditions and throughout growth in *M. xanthus*[16]. Collectively, our data show that Ap4A inhibits IMPDH *in vitro* at concentrations that roughly match those present *in vivo*.

**Ap4A binds to the CBS domains of IMPDH.**

Next, we determined the structure of Ap4A-bound *Bs*IMPDH (**Table 1**). *Bs*IMPDH consists of the catalytic triose isomerase (TIM)-barrel with two cystathionine-β-synthase (CBS) domains forming the disc-like Bateman module inserted into the TIM-barrel (**Figs. 2a**, **b**, **c**, **Extended Data Fig. 3a**). Four IMPDH molecules form a tetramer through their catalytic domains with each CBS domain pointing outward from the center of the tetramer (**Fig. 2b**). Electron density, which could be unambiguously attributed to Ap4A, was present in between the two CBS domains of each IMPDH monomer (**Extended Data Fig. 3b**). It binds into a cleft formed by the two CBS domains constituting the Bateman module (**Fig. 2c**, **Extended Data Fig. 3c**). Binding of Ap4A to *Bs*IMPDH closely resembles that of Ap5G bound to *A. gossypii* IMPDH[26] as well as that of the adenosine nucleoside moieties of two ATP molecules bound to *P. aeruginosa* IMPDH[25] (**Extended Data Fig. 3d**).

The crystal structures of the IMPDH Apo states from *B. anthracis*, *P. aeruginosa*, and *A. gossypii* show a high degree of disorder in their CBS domains, which diminishes in the presence of a ligand (**Extended Data Fig. 4**). Thus, we probed the impact of Ap4A and ATP (as control) on the conformational flexibility of *Bs*IMPDH by hydrogen/deuterium exchange-mass spectrometry (HDX-MS). Decrease in HDX with either ligand was exclusively present in the

CBS domains substantiating binding to this entity (**Extended Data Fig. 5a**). The progression of HDX in peptides from the CBS1 (residues 113-136) and CBS2 (residues 172-200) domains of the Bateman module evidenced bimodal distributions of deuterated peptide ions (**Extended Data Figs. 5b-d**), which are thought to arise from partial unfolding or conformational flexibility[27,28]. Bimodal behavior is less pronounced in the presence of Ap4A and ATP suggesting ligand-induced rigidification of the CBS domains. Thus, Ap4A and ATP restrict the conformational flexibility of the CBS domains of IMPDH.

**Ap4A induces formation of a less active IMPDH octamer.**

Bacterial IMPDH enzymes are grouped into classes I and II depending on their oligomeric states and catalytic properties[29]. Class I enzymes (e.g. *Pa*IMPDH) are octameric irrespective of their bound ligand, exhibit comparably low but positive cooperative enzymatic activity, and increased catalytic efficiency accompanied by loss of cooperativity when ATP is present[25]. Class II enzymes (e.g., *Bs*IMPDH) can be tetrameric (apo or IMP-bound) or octameric ($NAD^+$ or ATP-bound). Both states show Michaelis-Menten-like kinetic properties[29]. Our biochemical experiments revealed that Ap4A and ATP, albeit binding with approximately 700-fold different affinity, share their interaction site in the CBS domains and similarly restrict its conformational flexibility. Thus, both ligands may affect the tetramer/octamer equilibrium of *Bs*IMPDH. If true, this also raises the question as to why Ap4A strongly restricts the enzymatic activity of *Bs*IMPDH while ATP does so only moderately, if at all (**Fig. 1f**).

Analysis of the crystal structure of Ap4A-bound *Bs*IMPDH suggests that two IMPDH tetramers engage into an octamer through their Ap4A-bound CBS domains (**Fig. 2d**). This *Bs*IMPDH octamer is stabilized by the arginines 141 and 144 of the CBS domains of one tetramer, which interact with the phosphates of the Ap4A molecules of the other tetramer, and *vice versa* (**Fig. 2e**). Thus, our structure suggests that Ap4A promotes the joining of two *Bs*IMPDH tetramers *via* their CBS domains into an octamer.

Next, we employed mass photometry, which enables direct mass determination of single molecules in solution by interferometric scattering microscopy[30]. In the absence of substrates, *Bs*IMPDH predominantly appeared as tetramer, the portion of which is further enlarged in the presence of $NAD^+$ and IMP (**Figs. 2f**, **2g**). Ap4A promoted formation of *Bs*IMPDH octamers in a dose-dependent manner with $EC_{50}$ values of 90 µM and 6 µM in absence and presence of substrates, respectively (**Fig. 2g**, **Extended Data Figs. 6a**, **6b**). The addition of ATP enforced octamer formation with comparable $EC_{50}$ in the absence (i.e., 45 µM ATP) but with a roughly 250-fold higher $EC_{50}$ than that exhibited by Ap4A in the presence of substrates (**Fig. 2g**), in agreement with the higher inhibitory potence of Ap4A for *Bs*IMPDH activity (**Figs. 1f**, **h**). We presume that the discrepancies in $EC_{50}$ related to the presence of substrate are a consequence of their impact on the oligomerization state of the enzyme[29]. The observed fraction of *Bs*IMPDH octamers induced by other Ap*n*A and Ap*n*G dinucleotides and adenosine mononucleotides (**Fig. 2h**, **Extended Data Fig. 6f**) correlated well with their impact on enzymatic activity (**Figs. 1f-h**).

Guided by the structure (**Fig. 2e**), we conceived several variants that should not bind Ap4A anymore, i.e., K202A, R141A/R144A, and ΔCBS, in which the CBS domains from residues Val95 to Ile 208 were replaced by a Ser-Gly-Ser linker. The K202A variant was still able to octamerize in dependence on Ap4A albeit higher concentrations were required (**Fig. 2i**, **Extended Data Fig. 6c**), and showed a modest Ap4A-dependent reduction in activity (**Extended Data Figs. 2c**, **6g**). The R141A/R144A and ΔCBS variants were insensitive to Ap4A-dependent regulation in enzymatic activity (**Extended Data Figs. 2c**, **6a**) and tetramer-to-octamer equilibrium (**Fig. 2i**, **Extended Data Figs. 6d**, **6e**). The ΔCBS variants exhibited a higher $V_{max}$ of enzymatic activity than the wildtype (**Extended Data Figs**. **2c**, **6g**). Plotting the fraction of active sites residing in the octameric form versus the $V_{max}$ yielded a reasonable correlation, implying that the *Bs*IMPDH tetramer would exhibit a roughly 10-fold higher

activity than the octamer (**Extended Data Fig**. **6h**). Collectively, these data indicate that the promotion of *Bs*IMPDH octamers, which are enzymatically less active than the tetrameric form, represents the underlying mechanistic principle of Ap4A-dependent inhibition of *Bs*IMPDH activity. Of note, all assays were conducted at 25 °C for technical reasons instead of, e.g., 51 °C (*B. subtilis* heat shock temperature, see below). Nevertheless, we expect that these *in vitro* characteristics of IMPDH would also apply to the enzyme *in vivo*.

**Octamerization by Ap4A alters catalytic elements in IMPDH.**

Next, we wanted to understand why the Ap4A-induced octamer was catalytically less active than the tetramer. In solution employing HDX-MS we could not detect Ap4A-dependent changes in IMPDH's active site, marked by the catalytically essential cysteine residue 308[24], likely because of the high HDX rate of this region (peptides 297-308 and 297-310, see **SourceData**) or due to the enzyme fraction being octameric even in the absence of Ap4A (**Fig. 2f**). We thus made use of the exclusively tetrameric ΔCBS variant (**Fig. 3a**) and determined its crystal structure (**Table 1**). The structure of ΔCBS shows an identical tetrameric arrangement of the catalytic domains as the wildtype (**Fig. 3a**). In-depth comparison between the individual monomers of ΔCBS and Ap4A-bound *Bs*IMPDH revealed that the catalytic flap (i.e., Glu376-Glu398 and Phe413-Pro423) and the C-terminal residues (i.e., Gly467-Tyr485) were resolved in the ΔCBS structure, however not in that of the Ap4A-bound wildtype (**Fig. 3b**). Moreover, we spotted differences in the conformation of the active site loop containing the catalytic cysteine 308 (**Fig. 3c**). In the Ap4A-bound *Bs*IMPDH structure, this Cys308-containg loop points away from the catalytic site but orients towards the active center in the ΔCBS suited to execute its catalytic duty (**Fig. 3c**). Similar changes were also observed in the crystal structures of *P. aeruginosa* and *A. gossypii* IMPDH ΔCBS variants in the presence of the substrate IMP (**Extended data Fig. 7**), and the additional function of these in establishing IMPDH tetramer-to-tetramer interfaces (forming IMPDH octamers) implied that octamerization may influence IMPDH activity allosterically[31,32]. Collectively, our data suggest that the Ap4A-induced octamerization has direct consequences on the conformational geometry of the active site elements, and thus IMPDH activity.

**IMPDH and nucleotide metabolism in *B. subtilis*.**

To assesses whether our *in vitro* findings would have physiological relevance, we constructed a series of *B. subtilis* strains carrying mutations in the IMPDH-encoding gene *guaB* at its endogenous locus, using CRISPR-mediated gene editing. In the resulting mutant strains (K202A, the R141A/R144A double mutant, and ΔCBS) we examined the levels of adenosine and guanosine nucleotides as well as their precursors by liquid chromatography coupled to mass spectrometry (LC-MS). LC-MS profiling of *B. subtilis* grown at 30 °C revealed dysregulation of the purine nucleotide metabolism for all IMPDH mutant strains (**Fig. 4**). Specifically, the levels of IMP and its precursors PRPP, FGAR, and SAICAR were elevated, and similarly increased levels of XMP, GMP, GDP, and GTP, all of which derive from the IMPDH-dependent conversion of IMP to XMP, were apparent. In contrast, LC-MS suggested fewer perturbations in pools of adenylosuccinate and adenosine nucleotides. Collectively, the IMPDH mutants showed ~3- to 7-fold higher GTP:ATP ratios than the wild type, being in good agreement with our *in vitro* results. Collectively, our data suggest that dysregulation of IMPDH results in increased flux from the common ATP/GTP intermediate IMP towards GTP.

**IMPDH activity and *B. subtilis* heat tolerance.**

Given the profound effects of our IMPDH mutations on *B. subtilis* nucleotide metabolism at 30 °C (**Fig. 4**), we wondered whether these would translate to phenotypic differences at elevated temperatures that should promote Ap4A accumulation. Firstly, we grew wildtype *B. subtilis* and the mutant strains at 30 °C in liquid minimal medium (S7) whereupon the mutants displayed

a higher doubling time of approx. 46 min compared to 40 min for the wildtype during logarithmic growth, which probably results from their disarrayed metabolome (**Fig. 5a**). Secondly, to probe temperature resistance and tolerance (**Figs. 5b**, **5c**) phenotypes of the IMPDH mutant strains, the cultures grown to mid-log phase in S7 medium at 30 °C were used as inoculum for phenotypic characterization at elevated temperatures. On agar-plates incubated with serial dilutions at various temperatures (i.e., 22, 37, 45, 51 °C), the site-directed mutants and the ΔCBS strain displayed strongly compromised growth at 51 °C whereas at all other temperatures below 51 °C the mutants grew similarly as the wildtype cells. The K202A mutant, in contrast to R141A/R144A and ΔCBS, still afforded very weak growth even at 51 °C. These data indicate that the protective effect conferred by intact CBS domains for temperature resistance of *B. subtilis* is only required at higher temperatures (**Fig. 5b**). We furthermore investigated heat shock tolerance of our strains in liquid culture by rapidly shifting cells from 30 °C to 53 °C, a potentially lethal temperature inducing strong heat shock response[33]. Collectively, all investigated variants showed a mild trend towards lower survival rates than the wildtype strain although there was high variation in between the biological replicates (**Fig. 5c**). The K202A and R141A/R144A mutants were least affected and displayed a lower median of survival rate versus wildtype only after 60 min at 53 °C. This trend was more pronounced for the ΔCBS mutant strain. The gradation in the survival rates of the mutant strains coincides with the impact of Ap4A on oligomerization and activity of IMPDH variants *in vitro* (**Fig. 2j**, **Extended Data Fig. 6g**). We also quantified the intracellular Ap4A concentrations at 51 °C, showing a significant increase induced by heat shock (**Extended data Fig. 8**). These results suggest that regulation of IMPDH activity is critical to *B. subtilis* heat shock response.

# DISCUSSION

Ap4A is conserved across the domains of life[7]. In eukaryotes, Ap4A is involved in activating the microphthalmia-associated transcription factor during allergic-response-IgE[34,35] and inhibiting the cGAS-STING pathway[36]. Diverse dinucleotides can also serve as protective mRNA-caps during disulfide stress[37]. Even before the discovery of the molecular chaperones, Ap4A has been considered as heat stress signal[11], and been proposed to interact with DnaK, ClpB, and GroEL in *E. coli*[14,21]. Due to the lack of further targets, Ap4A was also considered as a metabolic waste product[38,8].

Here, we show that Ap4A interacts with and inhibits *Bs*IMPDH. IMPDH was previously identified as a target of Ap4A in *E. coli*[8,19] and in murine brain lysates[19], but this interaction was considered physiologically irrelevant, because Ap4A bound to *E. coli* IMPDH with only a five-fold higher affinity than ATP, the cellular concentration of which however is assumed to exceed that of Ap4A 5,000-fold[8]. Notably, IMPDHs from different organisms interact with different dinucleotides. Strength of these interactions and consequences on oligomerization state and activity vary considerably, e.g., *Pa*IMPDH binds Ap4A or ATP[8] and exhibits an octameric topology irrespective of the activity-stimulating ligand ATP[25]. The CBS of *A. gossypii* IMPDH possesses three nucleotide-binding sites, opposed to two in most other IMPDHs[32,39]. It binds ATP, GDP and Ap5G well, however Ap4A only with low affinity[26]. An open octamer of *A. gossypii* IMPDH with higher enzymatic activity is induced by ATP while GDP promotes a compacted octamer with diminished activity[39,40]. Our analysis of *Bs*IMPDH shows that adenosine dinucleotides (Ap*n*A), and to a lesser extent also ATP, but not mixed adenosine/guanosine dinucleotides (Ap*n*G) enforce formation of catalytically inactive octamers. Differences in IMPDH regulation seem compounded by the structural plasticity of their CBS domains[41]. This plasticity enables specific binding of different ligands, e.g., mononucleotides, dinucleotides, S-adenosyl-methionine, or NAD, in different enzyme (sub-)families[42].

IMPDH functions at a step where the synthetic routes for adenosine and guanosine nucleotides branch at the conversion of IMP to XMP, which subsequently serves as substrate

for guanosine nucleotides (**Fig. 4**). Disrupting CBS-dependent inhibition of IMPDH activity in *B. subtilis* led to elevated GMP, GDP and GTP. GTP concentration can have a significant role in *B. subtilis* stress resistance[43], and GTP depletion downregulates transcription of ribosomal RNA[44]. Thus, regulation of IMPDH activity might indirectly affect translation via GTP biosynthesis. Heat can induce protein unfolding/aggregation requiring chaperones to facilitate protein refolding or removal. Therefore, slowing translation could prevent cells from overwhelming the molecular chaperones with both the heat-induced protein aggregation and the demand of nascent protein folding, thereby promoting cellular survival. On the other side, downregulation of the guanosine nucleotides' *de novo* biosynthesis through CBS domain-dependent repression of IMPDH might favor the conversion of IMP to ATP, required for ATP-dependent chaperone and protein degradation systems.

Our data suggest that IMPDH regulation affects nucleotide metabolite homeostasis. Given the shared binding sites of ATP and Ap4A at the IMPDH CBS domains, we cannot rule out the possibility that ATP, either by itself or through competition with Ap4A, also interacts with IMPDH and that our mutations impeded this potential ATP-dependent regulation. However, the $K_d$'s of Ap4A and ATP for *Bs*IMPDH differ by 700-fold, and an intracellular Ap4A concentration of ~24 µM would be sufficient to restrict *Bs*IMPDH activity *in vivo* in light of literature reports on cellular Ap4A levels and stress-dependent induction in some bacterial species: *E. coli* 0.2 µM (basal)[8] or 2.4 µM (basal)[45] to 270 µM (104 µg/ml cadmium sulfate after 160 min)[46] and 750 µM (shift from 37-50 °C after 120 min)[46], *S. typhimurium* <0.3 µM (basal) to 168 µM (180 µg/ml diamide after 50 min) and 365 µM (110 µg/ml cadmium chloride after 30 min)[10], *S. typhimurium* 1 µM (basal) to 30 µM (shift from 28-50 °C after 50 min)[11]. Notably, overexpression of a (p)ppGpp synthetase in *B. subtilis* increased Ap4A 4-fold, hinting at crosstalk between Ap4A and (p)ppGpp[47].

Based on our data, we hypothesize that the reduced fitness of *B. subtilis* strains with de-regulated IMPDH during heat shock (**Figs. 5b**,**c**), which is accompanied by an Ap4A increase, should be primarily linked to the dinucleotide and only to a lesser extent to ATP. While further research on the conserved nature of the Ap4A-dependent regulation of IMPDH is needed, we propose Ap4A as central and conserved regulator in nucleotide metabolism.

# ONLINE METHODS

**Cloning of native and varied *Bs*IMPDH.** The genes encoding full-length *Bacillus subtilis* (*Bs*) IMPDH (*guaB*) or *Bs*IMPDH-ΔCBS were amplified by polymerase chain reaction (PCR) using chromosomal DNA of the *B. subtilis* NCIB3610 Δ*comI* strain[48] as template. Primers are listed in **Supplementary Table 2**. PCR products for mutated *Bs*IMPDH were generated by overlapping PCR. PCR products were cloned into pET-24d(+) plasmid (Novagen) using standard cloning techniques. *B. subtilis* lysyl-tRNA synthetase (LysRS) was amplified by PCR from the same template and introduced into pET-24d(+) plasmid (Novagen) encoding for an N-terminal hexahistidine-tagged protein.

**Synthesis of $^{32}$P-labelled Ap4A.** Radiolabelled Ap4A was synthesized with LysRS from *B. subtilis*. The protein was overexpressed in *E. coli* BL21(DE3) cells in lysogeny broth (LB) medium supplemented with 50 µg/ml kanamycin and 0.5 mM IPTG (added at $OD_{600}$ of approximately 0.5) at 20 °C for 16 hours. The pelleted cells (3,500 x *g*, 20 min, 4 °C) were resuspended in lysis buffer (20 mM HEPES-Na pH 8.0, 20 mM KCl, 20 mM $MgCl_2$, 250 mM NaCl, 20 mM imidazole) supplemented with protease inhibitors and DNaseI, and lysed by French Press. The lysate was run through a 1 ml HisTrap FF column (Cytiva) and eluted with a gradient of imidazole up to 500 mM. Fractions containing LysRS were dialyzed into fresh lysis buffer supplemented with TEV protease (50 mM Tris-Cl pH 8.0, 1 mM DTT, 0.5 mM EDTA, 150 mM NaCl) and applied to a 1 ml HisTrap FF column (Cytiva) to obtain the cleaved protein, which was dialyzed against SEC buffer (20 mM HEPES-Na pH 8.0, 20 mM KCl, 20

mM $MgCl_2$, 200 mM NaCl) overnight. LysRS was applied to a HiPrep 26/60 Sephacryl S-200 HR column (Cytiva) in SEC buffer to remove TEV. The protein was concentrated and stored in SEC buffer supplemented with 10% (v/v) glycerol.

To synthesize radiolabelled Ap4A, purified *B. subtilis* LysRS was incubated at final concentration of 10 µM in 20 mM HEPES-Na pH 8.0, 20 mM KCl, 20 mM $MgCl_2$, 200 nM $ZnCl_2$, 1.7 U/ml *E. coli* inorganic pyrophosphatase, 8 µCi $^{32}$P-γ-ATP and 2 mM non-radiolabelled ATP. Lastly, 1 mM lysine was added to initiate the reaction. The reaction was incubated at 37 °C and after 5 h quenched by addition of formic acid (0.33 M final). These conditions typically resulted in >70% conversion to Ap4A being a mix of labeled and unlabeled Ap4A. Ap4A was purified using a method adapted from Johnstone & Farr[14] with AEX buffer A (50 mM $NH_4HCO_3$ pH 8.6) and AEX buffer B (700 mM $NH_4HCO_3$ pH 8.6). A 1 ml HiTrap QFF anion exchange chromatography column (Cytiva) was equilibrated with 10 column volumes (CV) of AEX Buffer A and the Ap4A reaction, diluted 1:10 in AEX buffer A, loaded onto the column. The column was washed with 10 CV AEX buffer A followed by a ramp of 0-20% B over 10 CV, 20-40% B over 15 CV, 40-55% B over 10 CV and 55-100% B over another 10 CV, all at 1 ml/min flow rate. Elution fractions (1 ml) were analyzed by thin-layer chromatography as described[19] on PEI cellulose plates (Millipore) with 3 M $(NH_4)_2SO_4$ + 2% (w/v) EDTA as mobile phase. Plates were exposed to a phosphor screen and scanned on a Typhoon scanner. Pyrophosphate eluted upon wash with AEX buffer A, ATP eluted at the 20-40% B step, and Ap4A eluted at the 40-55% B step. Fractions that contained at least 98% pure Ap4A were pooled and used for the DRaCALA screen. The final Ap4A probe solution had an estimated concentration of 0.66 mM.

**DRaCALA.** The *Bacillus anthracis* Gateway Clone set overexpression libraries with carbenicillin and gentamicin resistance cassettes were constructed and lysates with overexpressed proteins were obtained as described previously[23]. Screening for binding targets of Ap4A was conducted by differential radial capillary action of ligand assay (DRaCALA)[22]. $^{32}$P-labelled Ap4A was diluted to 15 µM total concentration in binding buffer (10 mM Tris-Cl pH 7.5, 100 mM NaCl, 5 mM $MgCl_2$), added to lysates at an equal volume, incubated for 10 min with shaking, and then spotted onto nitrocellulose paper. The spotted DRaCALA reactions were exposed to a phosphoscreen and imaged with Typhoon scanner.

**Expression and purification of *Bs*IMPDH.** *Bs*IMPDH proteins were produced in *E. coli* BL21(DE3) in LB medium supplemented with 12.5 g/l D(+)-lactose-monohydrate, 50 µg/ml kanamycin for 14 h at 30 °C. Cells were harvested by centrifugation (3,500 x *g*, 20 min, 4 °C), suspended in buffer A (20 mM HEPES-Na pH 8.0, 250 mM NaCl, 20 mM KCl, 20 mM $MgCl_2$, and 40 mM imidazole) and lysed through an LM10 microfluidizer (Microfluidics) at 12,000 psi. Lysate was treated for 1 h at room temperature with TURBO DNase (Thermo Fisher Scientific) and then centrifuged (47,850 x *g*, 30 min, 4 °C). Supernatant was loaded onto a HisTrap HP 5 ml column (Cytiva) equilibrated with buffer A. After washing with 10 column volumes (CV) buffer A, *Bs*IMPDH was eluted with 4 CV buffer B (20 mM HEPES-Na pH 8.0, 250 mM NaCl, 20 mM KCl, 20 mM $MgCl_2$, and 250 mM imidazole). *Bs*IMPDH was concentrated (Amicon Ultracel-30K (Millipore)) to 1 ml and applied to SEC (HiLoad 26/600 Superdex 200 pg, Cytiva) equilibrated with 20 mM HEPES-Na pH 7.5, 200 mM NaCl, 20 mM KCl and 20 mM $MgCl_2$. *Bs*IMPDH-containing fractions were concentrated (Amicon Ultracel-30K (Millipore)) and snap-frozen in liquid nitrogen. *Bs*IMPDH concentration was quantified photometrically (NanoDrop Lite, Thermo Fisher Scientific) with extinction coefficients at 280 nm of *Bs*IMPDH variants and *Bs*IMPDH-ΔCBS of 21,890 and 18,910 $M^{-1} * cm^{-1}$, respectively.

**Isothermal titration calorimetry (ITC).** ITC experiments were performed at 25 °C with a MicroCal PEAQ-ITC instrument (Malvern Panalytical). The cell was filled with 25 µM of

purified *Bs*IMPDH and titrated with different concentrations of nucleotides to reach ligand saturation. Nucleotides were purchased from Jena Bioscience (purity of ≥95%). *Bs*IMPDH and ligands were diluted in the same buffer: 20 mM HEPES-Na pH 7.5, 200 mM NaCl, 20 mM KCl, and 20 mM $MgCl_2$. The titrations were performed with a first injection of 0.3 µl or 0.4 µl, which aims to remove potential air bubbles in the syringe and is being discarded from later analysis, followed by 18 injections of 2 µl each for the Ap4A titration or 12 injections of 3 µl each for all the other tested nucleotides. Data were processed with the MicroCal PEAQ-ITC Analysis Software (Malvern Panalytical) and fitted with the 'Single set of identical sites' model.

**Assays for *Bs*IMPDH activity.** All measurements were conducted with 100 nM *Bs*IMPDH in 100 mM Tris-Cl pH 8.0, 100 mM KCl and 2 mM DTT at 25 °C. All except one assay were conducted with $NAD^+$ (Sigma Aldrich, ≥95% by HPLC) concentration kept constant at 3 mM and IMP (Sigma Aldrich, ≥99% by HPLC) employed in variable concentrations (25, 50, 100, 200, 400, 600, 800, 1,000 µM). In one assay (**Fig. 1e**), IMPDH activity was quantified at constant IMP concentration (3 mM), and $NAD^+$ employed in variable concentrations (25, 50, 100, 250, 500, 1,000, 2,500, 5,000 µM). Where denoted, nucleotides were supplemented with final concentrations of 1 µM, 3 µM 10 µM, 30 µM, and 100 µM (Ap4A), 10 µM (Ap3A, Ap5A, Ap6A, Ap3G, Ap4G, Ap5G), or 2 mM (AMP, ADP, ATP) as indicated in the figures.
Enzymatic reactions were started by the addition of *Bs*IMPDH, and the velocity of product formation was quantified by increase in absorbance at 340 nm originating from the NADH product in a microplate reader (EPOCH2, BioTek). Analysis of *Bs*IMPDH enzyme kinetic parameters was performed with the software GraphPad Prism version 6.0.1.

**Hydrogen/deuterium exchange mass spectrometry (HDX-MS).** Prior HDX-MS, *Bs*IMPDH was mixed with Ap4A or ATP to reach final concentrations of 50 µM and 5 mM, respectively. HDX-MS experiments were conducted and analyzed as described previously aided by a two-arm robotic autosampler (LEAP Technologies)[49]. In brief, 7.5 µl of *Bs*IMPDH solution were mixed with 67.5 µl of $D_2O$-containing SEC buffer (20 mM HEPES-Na pH 7.5, 20 mM $MgCl_2$, 20 mM KCl, 200 mM NaCl) to start the exchange reaction. After 10, 30, 95, 1,000 or 10,000 s of incubation at 25 °C, samples of 55 µl were taken from the reaction and mixed with an equal volume of quench buffer (400 mM $KH_2PO_4/H_3PO_4$, 2 M guanidine-HCl, pH 2.2) kept cold at 1 °C. 95 µl of the resulting mixture were injected into an ACQUITY UPLC M-Class System with HDX Technology (Waters)[50]. Undeuterated samples were prepared similarly by 10-fold dilution in $H_2O$-containing SEC buffer. *Bs*IMPDH was digested online with immobilized porcine pepsin at 12 °C under a constant flow (100 µl/min) of water + 0.1% (v/v) formic acid and the resulting peptic peptides collected on a trap column (2 mm x 2 cm) kept at 0.5 °C that was filled with POROS 20 R2 material (Thermo Fisher Scientific). After 3 min, the trap column was placed in line with an ACQUITY UPLC BEH C18 1.7 µm 1.0 x 100 mm column (Waters), and the peptides eluted at 0.5 °C using a gradient of water + 0.1% (v/v) formic acid (A) and acetonitrile + 0.1% (v/v) formic acid (B) at 30 µl/min flow rate as follows: 0-7 min/95-65% A, 7-8 min/65-15% A, 8-10 min/15% A. Peptides were ionized by electrospray ionization (capillary temperature 250 °C, spray voltage 3.0 kV) and mass spectra acquired from 50-2,000 m/z on a G2-Si HDMS mass spectrometer with ion mobility separation (Waters) in enhanced high definition MS ($HDMS^E$) or high definition MS (HDMS) mode for undeuterated and deuterated samples, respectively[51,52]. [Glu1]-Fibrinopeptide B standard (Waters) was employed for lock mass correction. During each run, the pepsin column was washed three times with 80 µl of 4% (v/v) acetonitrile and 0.5 M guanidine hydrochloride and blanks were performed between each sample. Three technical replicates (independent HDX reactions) were measured per incubation time.
Peptides were identified with ProteinLynx Global SERVER 3.0.1 (PLGS, Waters) from the non-deuterated samples acquired with $HDMS^E$ by employing low energy, elevated energy, and

intensity thresholds of 300, 100 and 1,000 counts, respectively. Ions were matched to peptides with a database containing the amino acid sequences of *Bs*IMPDH, porcine pepsin and their reversed sequences with the following search parameters: peptide tolerance = automatic; fragment tolerance = automatic; min fragment ion matches per peptide = 1; min fragment ion matches per protein = 7; min peptide matches per protein = 3; maximum hits to return = 20; maximum protein mass = 250,000; primary digest reagent = non-specific; missed cleavages = 0; false discovery rate = 100. Deuterium incorporation into peptides was quantified with DynamX 3.0 software (Waters). Only peptides that were identified in all undeuterated samples and with a minimum intensity of 25,000 counts, a maximum length of 25 amino acids, a minimum number of two products with at least 0.1 product per amino acid, a maximum mass error of 25 ppm and retention time tolerance of 0.5 minutes were considered for analysis. All spectra were manually inspected and, if necessary, peptides omitted (e.g., in case of low signal-to-noise ratio or presence of overlapping peptides). Parameters of the HDXMS experiments are in **Supplementary Table 1**. Raw data are in **Source Data** (provided as Excel file).

**Protein crystallization, X-ray diffraction and structure determination.** *Bs*IMPDH was crystallized at 20 °C by sitting drop vapor diffusion. For Ap4A-bound *Bs*IMPDH, 250 µM of *Bs*IMPDH was incubated with 2 mM Ap4A for 10 min at 20 °C. For *Bs*IMPDH-ΔCBS, 250 µM protein solution was employed. Crystallization screens was performed in SWISSCI MRC 2-well plates (Jena Bioscience) with a reservoir volume of 30 µl by mixing 0.25 µl of protein with an equal volume of precipitant solution. Crystals were obtained after 2 days. Optimization-screens were carried out as hanging drop with a reservoir of 1 ml by adding 1 µl precipitant solution to 1µl of protein solution. Ap4A-bound *Bs*IMPDH crystallized in 50 mM sodium acetate (pH 4.5) and 20% (v/v) 1,2-propanediol; *Bs*IMPDH-ΔCBS in 0.1 M sodium citrate pH 5.6, 0.2 M potassium/sodium tartrate and 2.0 M ammonium sulfate. Prior data collection, crystals were flash-frozen in liquid nitrogen after addition of 20% (v/v) glycerol. Data were collected under cryogenic conditions at ID23-1 of the European Synchrotron Radiation Facility (ESRF) and at P14.2 beamline of BESSY II[53]. Data were processed, reduced and merged with Mosflm[54] and AIMLESS[55]. Structures of Ap4A-bound *Bs*IMPDH and *Bs*IMPDH-ΔCBS were solved by molecular replacement with PHASER[56] and the *Pa*IMPDH (PDB-ID: 4DQW[25]) as search model. Structures were built in Coot[57], and refined with REFMAC5[58] and PHENIX refinement[59]. Figures were generated with PYMOL[60] and ChimeraX[61].

**Mass Photometry.** Oligomerization of *Bs*IMPDH was determined by mass photometry[30] using the One MP mass photometer (Refeyn). Buffer composition in all measurements was: 100 mM Tris-Cl pH 8.0, 100 mM KCl and 2 mM DTT. To calibrate the instrument, native protein standards (Biorad) were diluted 50-fold in sample buffer at room temperature. 2 µl of diluted calibration mixture was mixed with 18 µl of sample buffer in silicone wells on a cleaned microscope slide (170 ± 5 µm thickness, Marienfeld). We used the 66, 146, 480 and 1,048 kDa peaks of the standard proteins for a four-point calibration curve. For the measurements, 18 µl buffer was pre-loaded into a silicone well, then 2 µl of a 1,000 nM concentrated protein solution was mixed in prior to acquisition (100 nM *Bs*IMPDH final). $NAD^+$ and IMP were used at 3 mM final concentrations . We collected 6,000 frames for each sample using default instrument parameters. Data were analyzed with the DiscoverMP software provided by Refeyn, using default parameters with reflection and movement corrections for event extraction and fitting. Frames affected by strong vibration or aggregates moving across the image were manually excluded.

**Bacterial growth conditions and strain construction.** *In vivo* analyses were conducted using the non-domesticated *B. subtilis* NCBI3610 carrying the mutant *comI* Q12L[48] (3610, wildytpe). *B. subtilis* cultures were grown in S7 medium[47] at 30 °C. Mutant strains were constructed by

the CRISPR/Cas9 method[62] (**Supplementary Table 2**). Briefly, 5'- and 3'-ends of each repair template were amplified by PCR with one site-directed mutagenesis primer and one primer containing a unique BsaI cleavage site for Golden Gate assembly. 5'- and 3'-ends were amplified by overlap-extension PCR generating a mutant repair template flanked by two BsaI cleavage sites. Protospacers were designed and assembled as described[62], and each was designed with two unique BsaI cleavage sites for Golden Gate assembly. *E. coli* TOP10 chemically-competent cells were transformed with the Golden Gate reactions, the plasmids isolated and subsequently used for transformation of *E. coli* MC1061. Isolated plasmids from the latter were used for *B. subtilis* 3610 transformation[62]. Site-specific DNA sequencing confirmed mutants (**Supplementary Table 3**).

**LCMS quantification of metabolites.** *B. subtilis* strains were grown in S7 medium supplemented with 20 amino acids (20 µg/ml WY, 40 µg/ml C, 50 µg/ml ARNGQHILKMPSTVF, 500 µg/ml DE) at 30 °C until an $OD_{600}$ of 0.6. For metabolite extraction, 5 ml culture were filtered through a PTFE membrane (Sartorius). The membrane was submerged in 3 ml extraction solvent mix (50:50 (v/v) chloroform/water) kept on ice and mixed vigorously for 15 seconds. Extracts were centrifuged at 5,000 x *g* for 10 minutes at 4 °C, the aqueous phase removed and further centrifuged at 20,000 x *g* for 10 minutes at 4 °C. Samples were stored at -80 °C. Samples were run on an LC-MS/MS system (Q-exactive hybrid quadrupole-orbitrap mass spectrometer) equipped with an ACQUITY UPLC BEH C18 column (1.7 µm, 2.1 x 100 mm, Waters) in full-scan selected ion monitoring (MS-SIM) mode. MS parameters were: 70,000 resolution; automatic gain control of $10^6$; maximum injection time of 40 ms; scan range of 90-1,000 m/z. Analytes were eluted with a gradient of 97:3 (v/v) water/methanol, 10 mM tributylamine pH 8 (solvent A) and acetonitrile (solvent B) at 0.2 ml/min flow rate: 0-19 min/95-0% A, 19-24 min/0-95% A. Raw data were converted to mzXML format and quantification of metabolites was conducted using Metabolomics Analysis and Visualization Engine (MAVEN).
Normalized ion intensities of Ap4A were converted to intracellular concentrations as described[47] with $C_{Ap4A} = (V_{extract} * IC_{Ap4A} / E_{LCMS}) / (V_{culture} * OD * F_{cell})$, where $V_{extract}$ is the volume of the aqueous phase of the extract (1.5 ml); $IC_{Ap4A}$ is the ion intensity of Ap4A in the sample; $E_{LCMS}$ is the determined LC-MS detection efficiency of Ap4A (4.24 x $10^7$ counts per µM); $V_{culture}$ is the volume of the harvested culture; $OD$ is the $OD_{600}$ of the harvested culture; and $F_{cell}$ is the approximate fraction of cell volume in a normalized culture (0.00052 ml per 1 ml culture per $OD_{600}$). $F_{cell}$ was approximated based on *B. subtilis* density of 2.2 x $10^8$ CFU per ml per $OD_{600}$ unit and an intracellular volume of 2.38 fl (cell length of 4 µm and radius of 0.435 µm). Intracellular concentrations of Ap3A and Ap4G were determined by same procedure. Intracellular concentrations of AMP, ADP and ATP were determined similarly but employed the LC-MS detection efficiency of ATP (2 x $10^8$ counts per µM).

**Heat shock experiments.** *B. subtilis* strains were inoculated into S7 medium supplemented with 0.5% (w/v) casamino acids and grown at 30 °C until an $OD_{600}$ of 0.3-0.4. These cultures were inoculated into fresh media in a 96-well plate and grown in a plate reader (BioTek) at 30 °C with shaking for 16 hours. For measurement of heat resistance, aliquots were withdrawn from cultures of each strain, and serial dilutions thereof employed to spot agar-containing S7 plates for incubation overnight at 22, 37, 45, or 51 °C. Plates were photographed to examine the growth at each temperature. For measurement of heat tolerance, 50 µl of the cultures were used to inoculate a tube containing 2 ml S7 medium supplemented with 0.5% (w/v) casamino acids pre-warmed to 53 °C. Samples for enumeration of colony-forming units were withdrawn before heat shock (0 min) or after 15, 30, or 60 min of incubation under vigorous agitation and incubated on LB agar plates at 30 °C until countable colonies were obtained.

**Reporting summary**. Further information on research design is available in the Nature Research Reporting Summary linked to this article.

## Data availability

Structure factors and coordinates of X-ray crystallographic datasets have been deposited at the Protein Data Bank (www.rcsb.org) under the accession codes 7OJ1 and 7OJ2 for the Ap4A-bound *Bs*IMPDH and *Bs*IMPDH-ΔCBS, respectively. All other structural data employed in this manuscript (accession codes 3L2B, 3TSB, 4DQW, 4XTI, 4XWU, 5AHL, 5AHM, 5MCP, 6GJV, 6RPU) are publicly available in the Protein Data Bank. Source data are provided with this paper for figures 1, 2, 4, and 5, and for Extended data figures 1, 2, 5, 6, and 8.


## Acknowledgements

This work was supported by the priority program of the Deutsche Forschungsgemeinschaft (DFG) SPP1879 – "Nucleotide second messenger signaling in bacteria" (to GB), the USA National Institute of Health R35 GM127088 and the Howard Hughes Medical Institute Faculty Scholars Award (to JDW), and the National Science Foundation (NSF) grant award no. 1715710 (to DAN). We thank the European Synchrotron Radiation Facility (Grenoble, France) and the Electron Storage Ring BESSY II (Berlin, Germany) for the excellent beamline support. We acknowledge support from the "DFG-core facility for interactions, dynamics and macromolecular assembly structure" at the Philipps-University Marburg (to GB). GH acknowledges support from the Free-floater program of the Max Planck Society.


## Author contributions

Conceptualization: JDW, GB
Methodology: GH, DAN
Experimental investigation: PIG, MY, WS, CNM, JY, AP
Funding acquisition: JDW, GB
Supervision: JDW, GB
Writing – original draft: PIG, MY, WS, JDW, GB
Writing – review & editing: all authors read and commented on the manuscript.

## Competing interests

The authors declare no competing interests.

## Tables

Table 1

| | Ap4A-bound *Bs*IMPDH | *Bs*IMPDH-ΔCBS |
|---|---|---|
| **Data collection** | | |
| Space group | I4 | I422 |
| Cell dimensions | | |
| | 133.75 | 110.91 |
| a, b, c (Å) | 133.75 | 110.91 |
| | 149.68 | 156.85 |
| α, β, γ (°) | 90 | 90 |

| | | |
|---|---|---|
| | 90 | 90 |
| | 90 | 90 |
| Wavelength (Å) | 0.978561 | 0.918400 |
| Resolution (Å) | 66.88 - 2.442 (2.53 - 2.442) | 45.28 - 1.76 (1.823-1.76) |
| $R_{merge}$ | 0.067 (0.2841) | 0.03072 (0.2892) |
| I / σI | 6.55 (2.58) | 13.79 (2.43) |
| Completeness (%) | 99.58 (99.82) | 99.95 (100.00) |
| Redundancy | 1.9 (1.9) | 2.0 (2.0) |
| CC1/2 | 0.992 (0.641) | 0.999 (0.708) |
| **Refinement** | | |
| Resolution (Å) | 66.88 - 2.442 | 45.28 - 1.76 |
| No. reflections | 48533 (4865) | 48580 (4794) |
| $R_{work}$ / $R_{free}$ | 0.27/0.29 | 0.17/0.19 |
| No. atoms | 6255 | 2868 |
| Protein | 6112 | 2868 |
| Ligand/ion | 108 | 17 |
| Water | 35 | 200 |
| B-factors | 71.44 | 29.89 |
| Protein | 70.65 | 29.45 |
| Ligand/ion | 120.22 | 36.30 |
| Water | 58.99 | 35.20 |
| R.m.s. deviations | | |
| Bond lengths (Å) | 0.006 | 0.016 |
| Bond angles (°) | 1.02 | 1.78 |
| Ramachandran | | |
| Favored (%) | 95.01 | 97.98 |
| Allowed (%) | 4.37 | 2.02 |
| Outliers (%) | 0.62 | 0.00 |

# Figure legends

**Fig. 1. Ap4A inhibits IMPDH in a non-competitive manner. a.** Scheme of Ap4A formation by lysyl-tRNA synthetase (Lys-RS) from ATP and lysyl-AMP (Lys-AMP). **b.** DRaCALA assay with $^{32}$P-labelled Ap4A employing a *B. anthracis* library suggests IMPDH as a target of Ap4A. **c.** Scheme of the enzymatic reaction catalyzed by IMPDH, the $NAD^+$-dependent conversion of IMP into XMP, which represent the starting points in the *de novo* biosynthesis of adenosine and guanosine nucleotides, respectively. **d.** Binding of adenosine nucleotides, and Ap*n*A and Ap*n*G dinucleotides (*n* = variable number of phosphates) to *Bs*IMPDH determined by isothermal titration calorimetry (ITC) and their intracellular concentrations determined by LC-MS. Asterisks denote bad binding curve fitting. LC-MS data represent the mean ± SD of n=3 biological replicates. The error of the $K_d$ derived from ITC data represents unambiguity in the curve fitting. **e-h.** Enzyme-kinetic behavior of *Bs*IMPDH for its conversion of the IMP substrate into XMP in dependence of **e.** Ap4A, **f.** adenosine nucleotides, **g.** Ap*n*G dinucleotides, and **h.** Ap*n*A dinucleotides. Individual data points of n=2 technical replicates are shown, and parameters of the fits are given in **Extended Data Fig. 2**.

**Fig. 2. Mechanism of the Ap4A-dependent inhibition of IMPDH. a.** Domain organization of IMPDH enzymes. The CBS domains forming a Bateman module (orange) are inserted into the catalytic domain (CD, green). **b.** Top view on the IMPDH structure bound to Ap4A, which binds into the CBS domains of the IMPDH oligomer. **c.** Close-up showing that Ap4A binds in a horseshoe-like manner into a cavity formed by the two CBS domains (Bateman module) of

an IMPDH monomer. **d.** Side view on the Ap4A-dependent IMPDH octamer showing that two tetramers of IMPDH form an octamer via their CBS domains. **e.** Close-up view onto a CBS module established by two IMPDH monomers belonging to different tetrameric rings. The interaction of the Bateman modules is mainly enforced by interactions between R141 and R144 residues of one monomer with the Ap4A bound in the Bateman module of the opposing monomer. **f-i.** Influence of substrates and ligands on the oligomeric state of *Bs*IMPDH (tetramer or octamer) analyzed by mass photometry. **f**, **i.** Representative distributions of tetrameric and octameric *Bs*IMPDH species for **f.** *Bs*IMPDH-WT, or **i.** *Bs*IMPDH CBS domain variants (K202A, R141A/R144A, ΔCBS), in dependence of substrates and/or ligands to the sample. Numbers in the diagrams reflect the molecular weight of the observed oligomeric species (mean ± SD) and their percentage of all observed molecules in the sample. **g, h, j.** The fraction of *Bs*IMPDH monomers in the octameric state in absence or presence of substrates displayed as a function of nucleotide or dinucleotide concentration. Individual data points of n=2 technical replicates are displayed, and their means used for curve-fitting. Where possible, $EC_{50}$ values (in μM) were derived from the dose-response curves.

**Fig. 3. Crystal structure and conformational changes in *Bs*IMPDH ΔCBS. a.** Cartoon representation of the crystal structures of *Bs*IMPDH-ΔCBS (blue, *left*), full-length *Bs*IMPDH (green and orange for the catalytic (CD) and CBS domains, respectively, *middle*), and the superimposition of both structures (*right*). *Bs*IMPDH-ΔCBS constitutes only one tetrameric ring through its catalytic domains opposed to CBS-dependent octamerization in full-length *Bs*IMPDH. **b.** The catalytic flap (red) and C-termini (orange) could be located in *Bs*IMPDH-ΔCBS (blue) but not full-length *Bs*IMPDH bound to Ap4A (white) evidencing a different conformation. **c.** Close-up view onto the Cys308-containing catalytic loop and catalytic flap regions of *Bs*IMPDH-ΔCBS (blue) and full-length *Bs*IMPDH in complex with Ap4A (red). The position of the IMP substrate was approximated based on an overlay with IMP-bound *P. aeruginosa* IMPDH-ΔCBS (PDB-ID: 5AHM[31]). Cys308 is dislocated in the Ap4A bound state but oriented towards the IMP substrate-binding site of *Bs*IMPDH-ΔCBS, thus likely representing the active conformation of IMPDH.

**Fig. 4. Mutations interfering with allosteric regulation of IMPDH activity perturb nucleotide metabolism of *B. subtilis*.** *In vivo* quantification of purine nucleotide metabolism intermediates in wildtype (WT) *B. subtilis* 3610 and IMPDH mutant strains. Data represent mean ± SD of n=3 biological replicates. The abbreviations are: PRPP, phosphoribosylpyrophosphate; FGAR, Phosphoribosyl-*N*-formylglycineamide; SAICAR, phosphoribosylaminoimidazolesuccinocarboxamide; IMP, inosine-5'-monophosphate; XMP, xanthosine-5'-monophosphate; GMP, GDP, GTP, guanosine-5'-mono-, di-, triphosphate; AMP, ADP, ATP, adenosine-5'-mono-, di-, triphosphate. The inset depicts a model of nucleotide metabolism and the regulation of *B. subtilis* IMPDH activity. Unpaired two-tailed t-tests were used to compare levels of metabolites for mutant strains versus WT. Asterisks indicate *p*-values: * $p \leq 0.05$, ** $p \leq 0.01$, *** $p \leq 0.001$; ns, not significant. Exact *p*-values are, PRPP: 0.0653 (WT vs. K202), 0.0740 (WT vs. R141A/R144A), 0.0079 (WT vs. ΔCBS); FGAR: 0.0744 (WT vs. K202), 0.0587 (WT vs. R141A/R144A), 0.0054 (WT vs. ΔCBS); SAICAR: 0.1206 (WT vs. K202), 0.0360 (WT vs. R141A/R144A), 0.0633 (WT vs. ΔCBS); IMP: 0.0743 (WT vs. K202), 0.0706 (WT vs. R141A/R144A), 0.0120 (WT vs. ΔCBS); XMP: 0.0468 (WT vs. K202), 0.0748 (WT vs. R141A/R144A), 0.0723 (WT vs. ΔCBS); GMP: 0.0382 (WT vs. K202), 0.2521 (WT vs. R141A/R144A), 0.1656 (WT vs. ΔCBS); GDP: 0.0435 (WT vs. K202), 0.0286 (WT vs. R141A/R144A), 0.0238 (WT vs. ΔCBS); GTP: 0.0003 (WT vs. K202), 0.1658 (WT vs. R141A/R144A), 0.0420 (WT vs. ΔCBS); Adenylosuccinate: 0.0849 (WT vs. K202), 0.0061 (WT vs. R141A/R144A), 0.0449 (WT vs. ΔCBS); AMP: 0.3275 (WT

vs. K202), 0.0895 (WT vs. R141A/R144A), 0.1809 (WT vs. ΔCBS); ADP: 0.1715 (WT vs. K202), 0.1095 (WT vs. R141A/R144A), 0.0112 (WT vs. ΔCBS); ATP: 0.8957 (WT vs. K202), 0.2897 (WT vs. R141A/R144A), 0.0332 (WT vs. ΔCBS); Ap4A: 0.1116 (WT vs. K202), 0.3522 (WT vs. R141A/R144A), 0.3207 (WT vs. ΔCBS).

**Fig. 5. Allosteric regulation of IMPDH activity is critical for tolerance of *B. subtilis* to heat shock conditions. a.** Doubling times of wildtype *B. subtilis* and IMPDH mutant strains in liquid S7 minimal medium at 30 °C during logarithmic growth phase. Data represent mean ± SD of n=4 biological replicates. Unpaired two-tailed t-tests were used to compare doubling times for mutant strains versus WT. Asterisks indicate *p*-values: ** $p \leq 0.01$. Exact *p*-values are: 0.0073 (WT vs. K202A), 0.0023 (WT vs. R141A/R144A), 0.0054 (WT vs. ΔCBS). **b-c.** Temperature-dependent growth of *B. subtilis* WT and IMPDH mutant strains. **b.** Serial dilutions of cultures from panel **a** were spotted on agar-containing S7 medium plates and incubated over night at the indicated temperatures. One representative experiment is depicted. **c.** Cultures grown at 30 °C were diluted in pre-warmed liquid S7 medium to reach 53 °C after mixing. Colony-forming units were enumerated from aliquots withdrawn after indicated incubation times. In the box plots, center lines represent median values, boxes the 25$^{th}$ and 75$^{th}$ percentiles, and whiskers the min and max values. Individual data points from n=6 (n=5 for ΔCBS) biological replicates are displayed as individual points.

**Table 1. Data collection and refinement statistics of crystallographic datasets.** Data were collected on ID23-1 (ESRF, Grenoble, France) and P14.2 (BESSY II, Berlin, Germany). Values in parentheses are for the highest-resolution shell.

## References


1. Steinchen, W. & Bange, G. The magic dance of the alarmones (p)ppGpp. *Molecular Microbiology* **101**, (2016).
2. Hauryliuk, V., Atkinson, G. C., Murakami, K. S., Tenson, T. & Gerdes, K. Recent functional insights into the role of (p)ppGpp in bacterial physiology. *Nature Reviews Microbiology* **13**, 298–309 (2015).
3. Hengge, R. High-Specificity Local and Global c-di-GMP Signaling. *Trends in Microbiology* (2021) doi:10.1016/j.tim.2021.02.003.
4. Jenal, U., Reinders, A. & Lori, C. Cyclic di-GMP: second messenger extraordinaire. *Nature reviews. Microbiology* **15**, 271–284 (2017).
5. Stülke, J. & Krüger, L. Cyclic di-AMP Signaling in Bacteria. *Annual Review of Microbiology* vol. 74 159–179 (2020).
6. Zamecnik, P. G., Stephenson, M. L., Janeway, C. M. & Randerath, K. Enzymatic synthesis of diadenosine tetraphosphate and diadenosine triphosphate with a purified lysyl-sRNA synthetase. *Biochemical and Biophysical Research Communications* **24**, 91–97 (1966).

7. Ferguson, F., McLennan, A. G., Urbaniak, M. D., Jones, N. J. & Copeland, N. A. Re-evaluation of Diadenosine Tetraphosphate (Ap4A) From a Stress Metabolite to Bona Fide Secondary Messenger. *Frontiers in Molecular Biosciences* **7**, 332 (2020).
8. Despotović, D. *et al.* Diadenosine tetraphosphate (Ap4A) – an E. coli alarmone or a damage metabolite? *FEBS Journal* **284**, 2194–2215 (2017).
9. Charlier, J. & Sanchez, R. Lysyl-tRNA synthetase from Escherichia coli K12. Chromatographic heterogeneity and the lysU-gene product. *The Biochemical journal* **248**, 43–51 (1987).
10. Bochner, B. R., Lee, P. C., Wilson, S. W., Cutler, C. W. & Ames, B. N. AppppA and related adenylylated nucleotides are synthesized as a consequence of oxidation stress. *Cell* **37**, 225–232 (1984).
11. Lee, P. C., Bochner, B. R. & Ames, B. N. AppppA, heat-shock stress, and cell oxidation. *Proceedings of the National Academy of Sciences* **80**, 7496 LP – 7500 (1983).
12. Nishimura, A. *et al.* Diadenosine 5',5'''-P1,P4-tetraphosphate (Ap4A) controls the timing of cell division in Escherichia coli. *Genes to cells : devoted to molecular & cellular mechanisms* **2**, 401–413 (1997).
13. Farr, S. B., Arnosti, D. N., Chamberlin, M. J. & Ames, B. N. An apaH mutation causes AppppA to accumulate and affects motility and catabolite repression in Escherichia coli. *Proceedings of the National Academy of Sciences of the United States of America* **86**, 5010–5014 (1989).
14. Johnstone, D. B. & Farr, S. B. AppppA binds to several proteins in Escherichia coli, including the heat shock and oxidative stress proteins DnaK, GroEL, E89, C45 and C40. *The EMBO journal* **10**, 3897–3904 (1991).
15. Ji, X. *et al.* Alarmone Ap4A is elevated by aminoglycoside antibiotics and enhances their bactericidal activity. *Proceedings of the National Academy of Sciences* **116**, 9578–9585 (2019).
16. Kimura, Y., Tanaka, C., Sasaki, K. & Sasaki, M. High concentrations of intracellular Ap4A and/or Ap5A in developing Myxococcus xanthus cells inhibit sporulation. *Microbiology (Reading, England)* **163**, 86–93 (2017).
17. Monds, R. D. *et al.* Di-adenosine tetraphosphate (Ap4A) metabolism impacts biofilm formation by Pseudomonas fluorescens via modulation of c-di-GMP-dependent pathways. *Journal of Bacteriology* **192**, 3011–3023 (2010).
18. Lundin, A. *et al.* The NudA protein in the gastric pathogen Helicobacter pylori is an ubiquitous and constitutively expressed dinucleoside polyphosphate hydrolase. *Journal of Biological Chemistry* **278**, 12574–12578 (2003).

19. Guo, W. *et al.* Isolation and identification of diadenosine 5′,5‴-P 1,P 4-tetraphosphate binding proteins using magnetic bio-panning. *Bioorganic and Medicinal Chemistry Letters* **21**, 7175–7179 (2011).
20. Azhar, M. A., Wright, M., Kamal, A., Nagy, J. & Miller, A. D. Biotin-c10-AppCH2ppA is an effective new chemical proteomics probe for diadenosine polyphosphate binding proteins. *Bioorganic & medicinal chemistry letters* **24**, 2928–2933 (2014).
21. Fuge, E. K. & Farr, S. B. AppppA-binding protein E89 is the Escherichia coli heat shock protein ClpB. *Journal of bacteriology* **175**, 2321–2326 (1993).
22. Roelofs, K. G., Wang, J., Sintim, H. O. & Lee, V. T. Differential radial capillary action of ligand assay for high-throughput detection of protein-metabolite interactions. *Proceedings of the National Academy of Sciences of the United States of America* **108**, 15528–15533 (2011).
23. Yang, J. *et al.* The nucleotide pGpp acts as a third alarmone in Bacillus, with functions distinct from those of (p) ppGpp. *Nature communications* **11**, 5388 (2020).
24. Hedstrom, L. IMP dehydrogenase: structure, mechanism, and inhibition. *Chemical reviews* **109**, 2903–2928 (2009).
25. Labesse, G. *et al.* MgATP regulates allostery and fiber formation in IMPDHs. *Structure* **21**, 975–985 (2013).
26. Fernández-Justel, D., Peláez, R., Revuelta, J. L. & Buey, R. M. The Bateman domain of IMP dehydrogenase is a binding target for dinucleoside polyphosphates. *Journal of Biological Chemistry* **294**, 14768–14775 (2019).
27. Weis, D. D., Wales, T. E., Engen, J. R., Hotchko, M. & Ten Eyck, L. F. Identification and Characterization of EX1 Kinetics in H/D Exchange Mass Spectrometry by Peak Width Analysis. *Journal of the American Society for Mass Spectrometry* **17**, 1498–1509 (2006).
28. Zhang, Z. & Smith, D. L. Determination of amide hydrogen exchange by mass spectrometry: a new tool for protein structure elucidation. *Protein science : a publication of the Protein Society* **2**, 522–531 (1993).
29. Alexandre, T., Rayna, B. & Munier-Lehmann, H. Two Classes of Bacterial IMPDHs according to Their Quaternary Structures and Catalytic Properties. *PLOS ONE* **10**, e0116578 (2015).
30. Young, G. *et al.* Quantitative mass imaging of single biological macromolecules. *Science* **360**, 423 LP – 427 (2018).
31. Labesse, G., Alexandre, T., Gelin, M., Haouz, A. & Munier-Lehmann, H. Crystallographic studies of two variants of Pseudomonas aeruginosa IMPDH with impaired allosteric regulation. *Acta crystallographica. Section D, Biological crystallography* **71**, 1890–1899 (2015).

760 32. Buey, R. M., Ledesma-Amaro, R., Balsera, M., de Pereda, J. M. & Revuelta, J. L. Increased riboflavin
761 production by manipulation of inosine 5'-monophosphate dehydrogenase in Ashbya gossypii. *Applied*
762 *microbiology and biotechnology* **99**, 9577–9589 (2015).
763 33. Schäfer, H. *et al.* The alarmones (p)ppGpp are part of the heat shock response of Bacillus subtilis. *PLOS*
764 *Genetics* **16**, e1008275 (2020).
765 34. Lee, Y.-N., Nechushtan, H., Figov, N. & Razin, E. The Function of Lysyl-tRNA Synthetase and Ap4A as
766 Signaling Regulators of MITF Activity in Fc_RI-Activated Mast Cells. *Immunity* **20**, 145–151 (2004).
767 35. Yannay-Cohen, N. *et al.* LysRS Serves as a Key Signaling Molecule in the Immune Response by
768 Regulating Gene Expression. *Molecular Cell* **34**, 603–611 (2009).
769 36. Guerra, J. *et al.* Lysyl-tRNA synthetase produces diadenosine tetraphosphate to curb STING-dependent
770 inflammation. *Science Advances* **6**, (2020).
771 37. Luciano, D. J., Levenson-Palmer, R. & Belasco, J. G. Stresses that Raise Np4A Levels Induce Protective
772 Nucleoside Tetraphosphate Capping of Bacterial RNA. *Molecular cell* **75**, 957-966.e8 (2019).
773 38. Baltzinger, M., Ebel, J. P. & Remy, P. Accumulation of dinucleoside polyphosphates in Saccharomyces
774 cerevisiae under stress conditions. High levels are associated with cell death. *Biochimie* **68**, 1231–1236
775 (1986).
776 39. Buey, R. M. *et al.* A nucleotide-controlled conformational switch modulates the activity of eukaryotic IMP
777 dehydrogenases. *Scientific Reports* **7**, 2648 (2017).
778 40. Buey, R. M. *et al.* Guanine nucleotide binding to the Bateman domain mediates the allosteric inhibition of
779 eukaryotic IMP dehydrogenases. *Nature Communications* **6**, (2015).
780 41. Ereño-Orbea, J., Oyenarte, I. & Martínez-Cruz, L. A. CBS domains: Ligand binding sites and
781 conformational variability. *Archives of biochemistry and biophysics* **540**, 70–81 (2013).
782 42. Anashkin, V. A., Baykov, A. A. & Lahti, R. Enzymes Regulated via Cystathionine β-Synthase Domains.
783 *Biochemistry. Biokhimiia* **82**, 1079–1087 (2017).
784 43. Kriel, A. *et al.* Direct regulation of GTP homeostasis by (p)ppGpp: a critical component of viability and
785 stress resistance. *Molecular cell* **48**, 231–241 (2012).
786 44. Krásný, L. & Gourse, R. L. An alternative strategy for bacterial ribosome synthesis: Bacillus subtilis rRNA
787 transcription regulation. *The EMBO journal* **23**, 4473–4483 (2004).
788 45. Plateau, P., Fromant, M., Kepes, F. & Blanquet, S. Intracellular 5',5'-dinucleoside polyphosphate levels
789 remain constant during the Escherichia coli cell cycle. *Journal of bacteriology* **169**, 419–422 (1987).

46. Coste, H., Brevet, A., Plateau, P. & Blanquet, S. Non-adenylylated bis(5'-nucleosidyl) tetraphosphates occur in Saccharomyces cerevisiae and in Escherichia coli and accumulate upon temperature shift or exposure to cadmium. *The Journal of biological chemistry* **262**, 12096–12103 (1987).
47. Fung, D. K., Yang, J., Stevenson, D. M., Amador-Noguez, D. & Wang, J. D. Small Alarmone Synthetase SasA Expression Leads to Concomitant Accumulation of pGpp, ppApp, and AppppA in Bacillus subtilis. *Frontiers in microbiology* **11**, 2083 (2020).
48. Konkol, M. A., Blair, K. M. & Kearns, D. B. Plasmid-encoded ComI inhibits competence in the ancestral 3610 strain of Bacillus subtilis. *Journal of bacteriology* **195**, 4085–4093 (2013).
49. Osorio-Valeriano, M. *et al.* ParB-type DNA Segregation Proteins Are CTP-Dependent Molecular Switches. *Cell* **179**, 1512-1524.e15 (2019).
50. Wales, T. E., Fadgen, K. E., Gerhardt, G. C. & Engen, J. R. High-speed and high-resolution UPLC separation at zero degrees Celsius. *Analytical chemistry* **80**, 6815–6820 (2008).
51. Geromanos, S. J. *et al.* The detection, correlation, and comparison of peptide precursor and product ions from data independent LC-MS with data dependant LC-MS/MS. *PROTEOMICS* **9**, 1683–1695 (2009).
52. Li, G.-Z. *et al.* Database searching and accounting of multiplexed precursor and product ion spectra from the data independent analysis of simple and complex peptide mixtures. *PROTEOMICS* **9**, 1696–1719 (2009).
53. Mueller, U. *et al.* The macromolecular crystallography beamlines at BESSY II of the Helmholtz-Zentrum Berlin: Current status and perspectives. *The European Physical Journal Plus* **130**, 141 (2015).
54. Powell, H. R., Battye, T. G. G., Kontogiannis, L., Johnson, O. & Leslie, A. G. W. Integrating macromolecular X-ray diffraction data with the graphical user interface iMosflm. *Nature protocols* **12**, 1310–1325 (2017).
55. Evans, P. R. & Murshudov, G. N. How good are my data and what is the resolution? *Acta crystallographica. Section D, Biological crystallography* **69**, 1204–1214 (2013).
56. McCoy, A. J. Solving structures of protein complexes by molecular replacement with Phaser. *Acta crystallographica. Section D, Biological crystallography* **63**, 32–41 (2007).
57. Emsley, P., Lohkamp, B., Scott, W. G. & Cowtan, K. Features and development of Coot. *Acta crystallographica. Section D, Biological crystallography* **66**, 486–501 (2010).
58. Murshudov, G. N. *et al.* REFMAC5 for the refinement of macromolecular crystal structures. *Acta Crystallographica Section D* **67**, 355–367 (2011).

59. Afonine, P. V *et al.* Towards automated crystallographic structure refinement with phenix.refine. *Acta Crystallographica Section D* **68**, 352–367 (2012).
60. Schrödinger, L. *The PyMOL Molecular Graphics System, Version 1.8*. (2015).
61. Pettersen, E. F. *et al.* UCSF ChimeraX: Structure visualization for researchers, educators, and developers. *Protein science : a publication of the Protein Society* **30**, 70–82 (2021).
62. Burby, P. E. & Simmons, L. A. CRISPR/Cas9 Editing of the Bacillus subtilis Genome. *Bio-protocol* **7**, (2017).
63. Tuominen, H. *et al.* Crystal structures of the CBS and DRTGG domains of the regulatory reagion of clostridium perfringens pyrophosphatase complexed with the inhibitor, AMP, and activator, diadenosine tetraphosphate. *Journal of Molecular Biology* **398**, 400–413 (2010).
64. Laskowski, R. A. & Swindells, M. B. LigPlot+: Multiple ligand-protein interaction diagrams for drug discovery. *Journal of Chemical Information and Modeling* **51**, 2778–2786 (2011).
65. Makowska-Grzyska, M. *et al.* Bacillus anthracis inosine 5'-monophosphate dehydrogenase in action: the first bacterial series of structures of phosphate ion-, substrate-, and product-bound complexes. *Biochemistry* **51**, 6148–6163 (2012).
66. Alexandre, T. *et al.* First-in-class allosteric inhibitors of bacterial IMPDHs. *European journal of medicinal chemistry* **167**, 124–132 (2019).

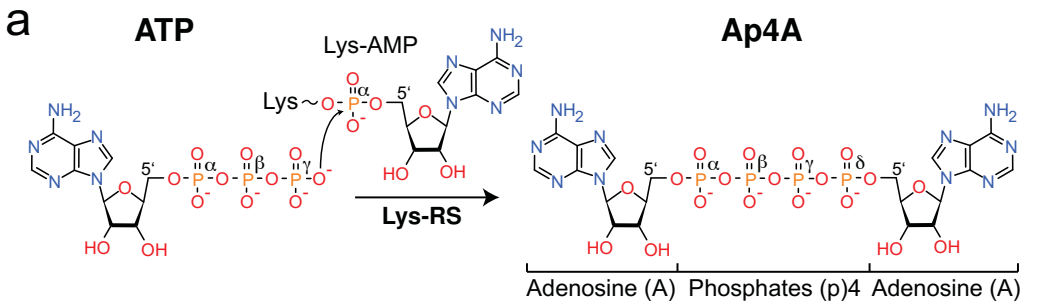


b

IMPDH (*B. anthracis*)

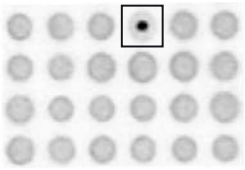

DRaCALA with [$^{32}$P]-Ap4A

c

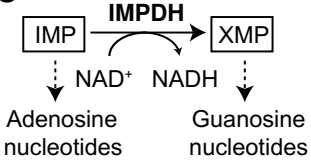


d

| Compound | | $K_d$ (μM) | *In vivo* (μM) |
|---|---|---|---|
| Adenosine | AMP | 17,900* | 97.9 ± 13.5 |
| | ADP | Not detected | 343.2 ± 53.1 |
| | ATP | 5,230* | 1,336 ± 199 |
| Ap*n*A | Ap3A | 62.0 ± 10.9 | 4.4 ± 0.5 |
| | Ap4A | 7.4 ± 2.1 | 24.2 ± 8.6 |
| | Ap5A | 30.4 ± 23.5 | Not detected |
| | Ap6A | 0.8 ± 0.2 | Not detected |
| Ap*n*G | Ap3G | Not detected | Not detected |
| | Ap4G | Not detected | 0.7 ± 0.4 |
| | Ap5G | Not detected | Not detected |

e

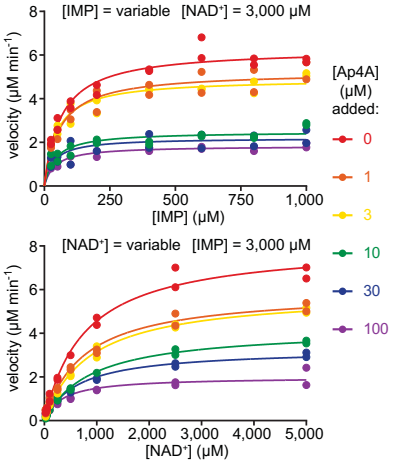


f

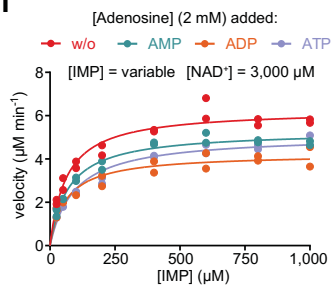


g

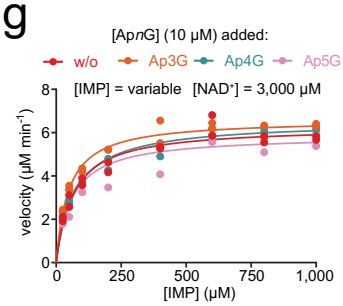


h

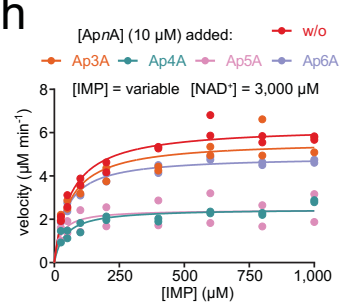

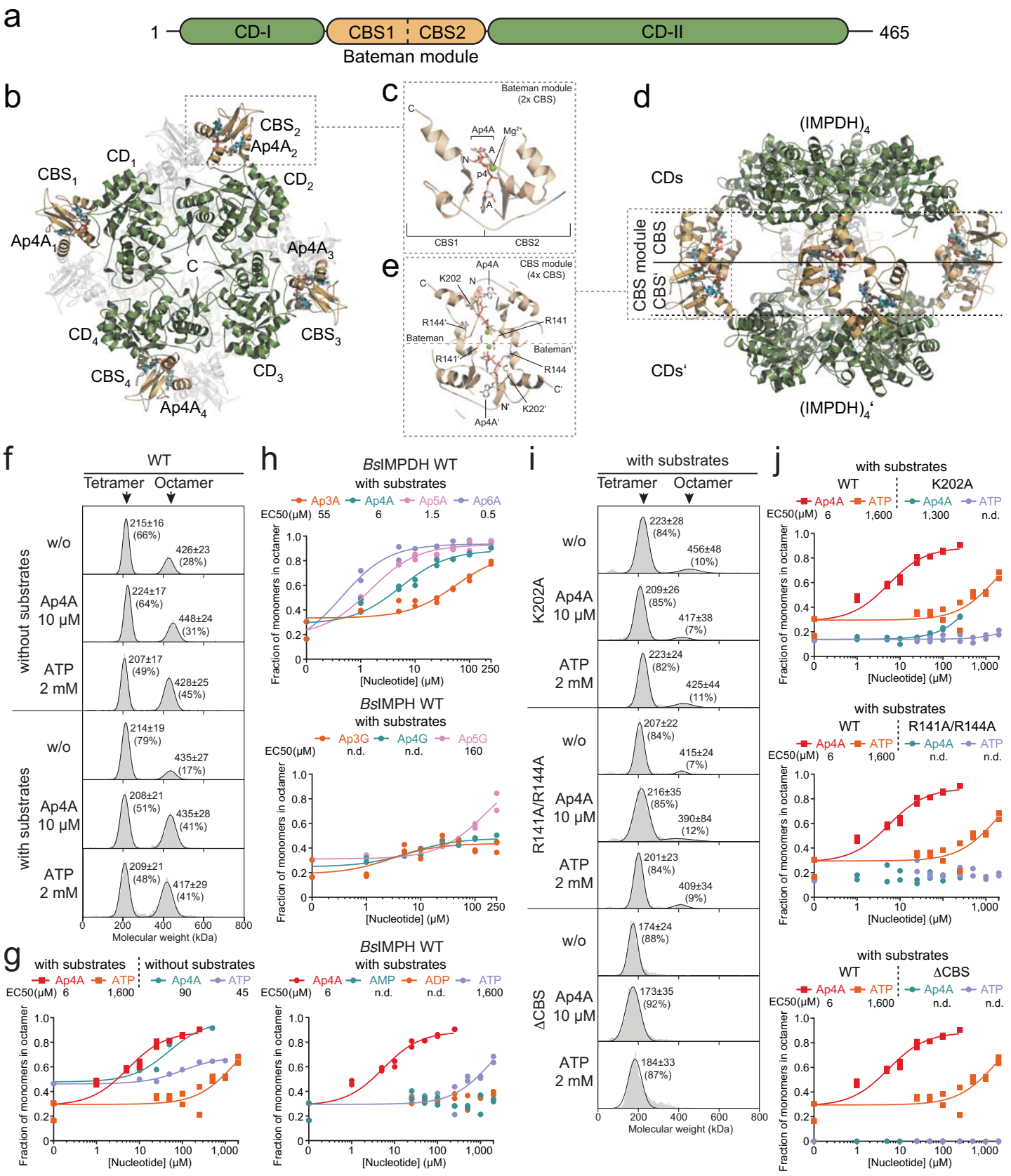
a
1
CD-I
CBS1
CBS2
CD-II
465
Bateman module
b
CBS2
Ap4A2
CD1
CBS1
CD2
Ap4A1
Ap4A3
C
CD4
CBS3
CBS4
CD3
Ap4A4
c
Bateman module
(2x CBS)
C
Ap4A
Mg2+
N
A
p4
A
CBS1
CBS2
d
(IMPDH)4
CDs
CBS module
CBS
CBS'
CDs'
(IMPDH)4'
e
Ap4A
CBS module
(4x CBS)
C
K202
N
R144'
R141
Bateman
R141'
Bateman'
R144
C'
N'
K202'
Ap4A'
f
WT
Tetramer
Octamer
without substrates
w/o
215±16
(66%)
426±23
(28%)
Ap4A
10 µM
224±17
(64%)
448±24
(31%)
ATP
2 mM
207±17
(49%)
428±25
(45%)
with substrates
w/o
214±19
(79%)
435±27
(17%)
Ap4A
10 µM
208±21
(51%)
435±28
(41%)
ATP
2 mM
209±21
(48%)
417±29
(41%)
0
200
400
600
800
Molecular weight (kDa)
g
with substrates
without substrates
Ap4A
ATP
Ap4A
ATP
EC50(µM) 6
1,600
90
45
Fraction of monomers in octamer
[Nucleotide] (µM)
Ap4A
AMP
ADP
ATP
EC50(µM) 6
n.d.
n.d.
1,600
h
BsIMPDH WT
with substrates
Ap3A
Ap4A
Ap5A
Ap6A
EC50(µM) 55
6
1.5
0.5
Fraction of monomers in octamer
[Nucleotide] (µM)
BsIMPH WT
with substrates
Ap3G
Ap4G
Ap5G
EC50(µM)
n.d.
n.d.
160
i
with substrates
Tetramer
Octamer
K202A
w/o
223±28
(84%)
456±48
(10%)
Ap4A
10 µM
209±26
(85%)
417±38
(7%)
ATP
2 mM
223±24
(82%)
425±44
(11%)
R141A/R144A
w/o
207±22
(84%)
415±24
(7%)
Ap4A
10 µM
216±35
(85%)
390±84
(12%)
ATP
2 mM
201±23
(84%)
409±34
(9%)
ΔCBS
w/o
174±24
(88%)
Ap4A
10 µM
173±35
(92%)
ATP
2 mM
184±33
(87%)
0
200
400
600
800
Molecular weight (kDa)
j
with substrates
WT
K202A
Ap4A
ATP
Ap4A
ATP
EC50(µM) 6
1,600
1,300
n.d.
Fraction of monomers in octamer
[Nucleotide] (µM)
with substrates
WT
R141A/R144A
Ap4A
ATP
Ap4A
ATP
EC50(µM) 6
1,600
n.d.
n.d.
with substrates
WT
ΔCBS
Ap4A
ATP
Ap4A
ATP
EC50(µM) 6
1,600
n.d.
n.d.

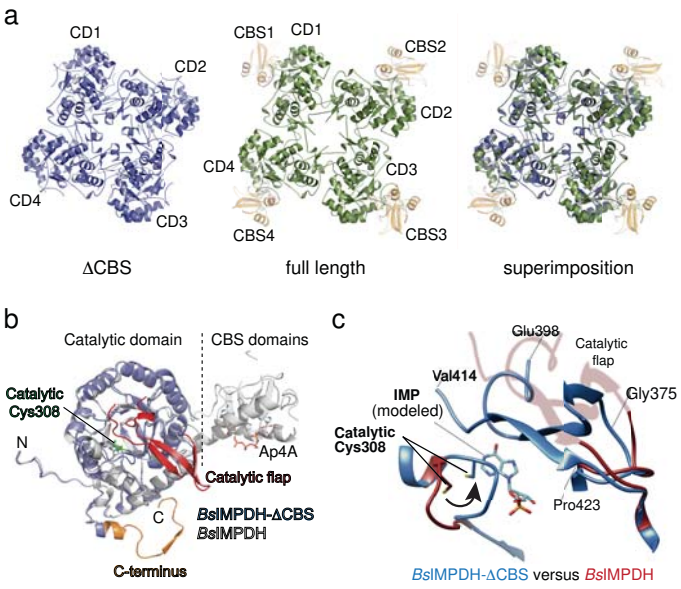
a
CD1
CD2
CD4
CD3
CBS1
CD1
CBS2
CD2
CD4
CD3
CBS4
CBS3
ΔCBS
full length
superimposition
b
Catalytic domain
CBS domains
Catalytic Cys308
N
Ap4A
Catalytic flap
C
BslMPDH-ΔCBS
BslMPDH
C-terminus
c
Glu398
Catalytic flap
Val414
IMP (modeled)
Gly375
Catalytic Cys308
Pro423
BslMPDH-ΔCBS versus BslMPDH

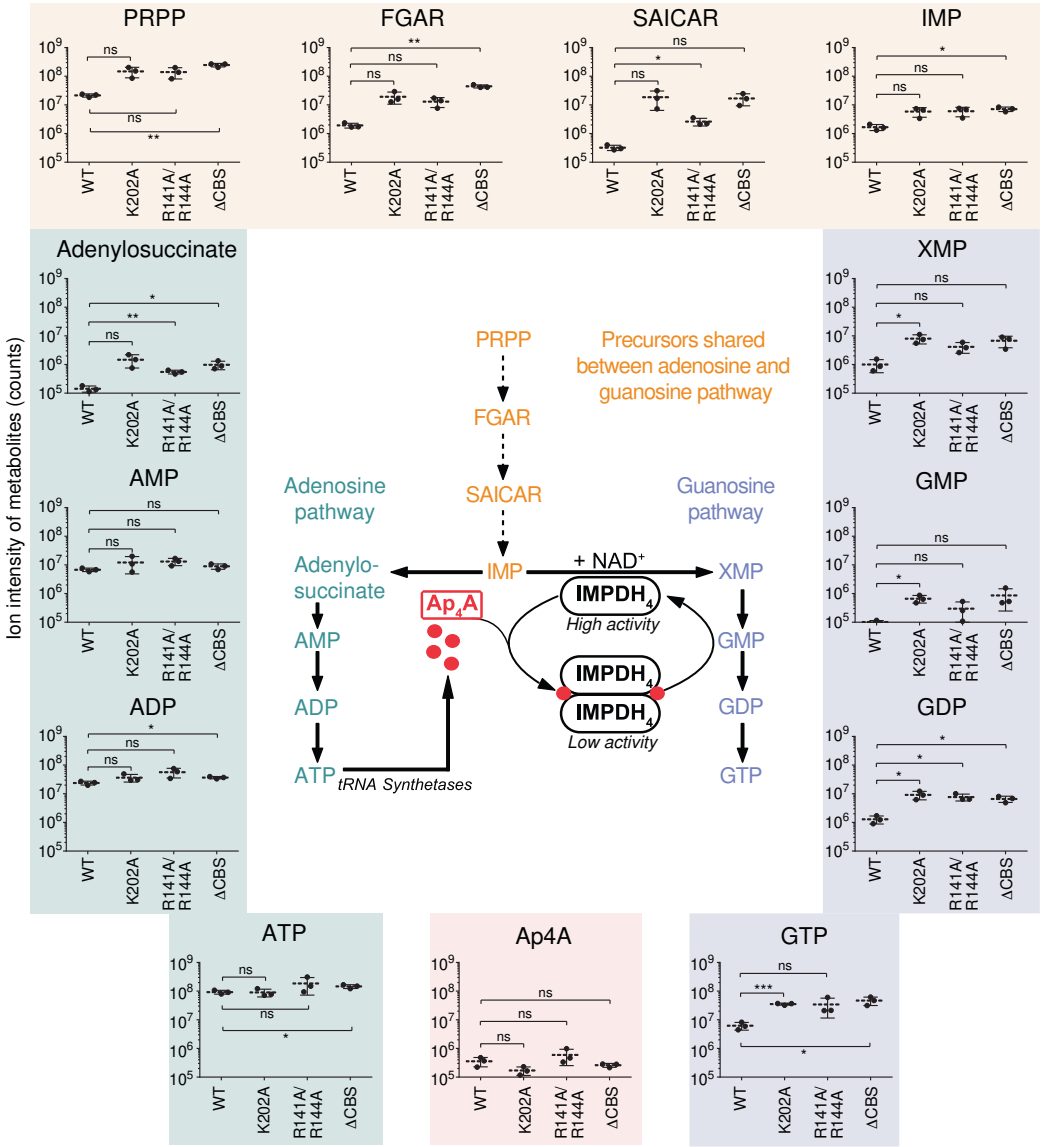
PRPP
FGAR
SAICAR
IMP
Adenylosuccinate
XMP
AMP
GMP
ADP
GDP
ATP
Ap4A
GTP
Ion intensity of metabolites (counts)
WT
K202A
R141A/R144A
ΔCBS
PRPP
FGAR
SAICAR
Adenosine pathway
Guanosine pathway
Precursors shared between adenosine and guanosine pathway
Adenylo-succinate
IMP
+ NAD+
XMP
AMP
Ap4A
IMPDH4
High activity
GMP
IMPDH4
IMPDH4
ADP
GDP
Low activity
ATP
tRNA Synthetases
GTP

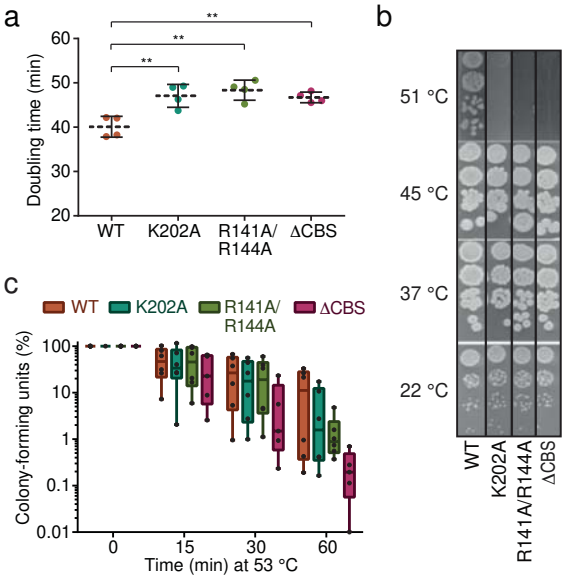
a
b
c
Doubling time (min)
60
50
40
30
20
**
**
**
WT
K202A
R141A/
R144A
ΔCBS
51 °C
45 °C
37 °C
22 °C
WT
K202A
R141A/R144A
ΔCBS
Colony-forming units (%)
100
10
1
0.1
0.01
0
15
30
60
Time (min) at 53 °C

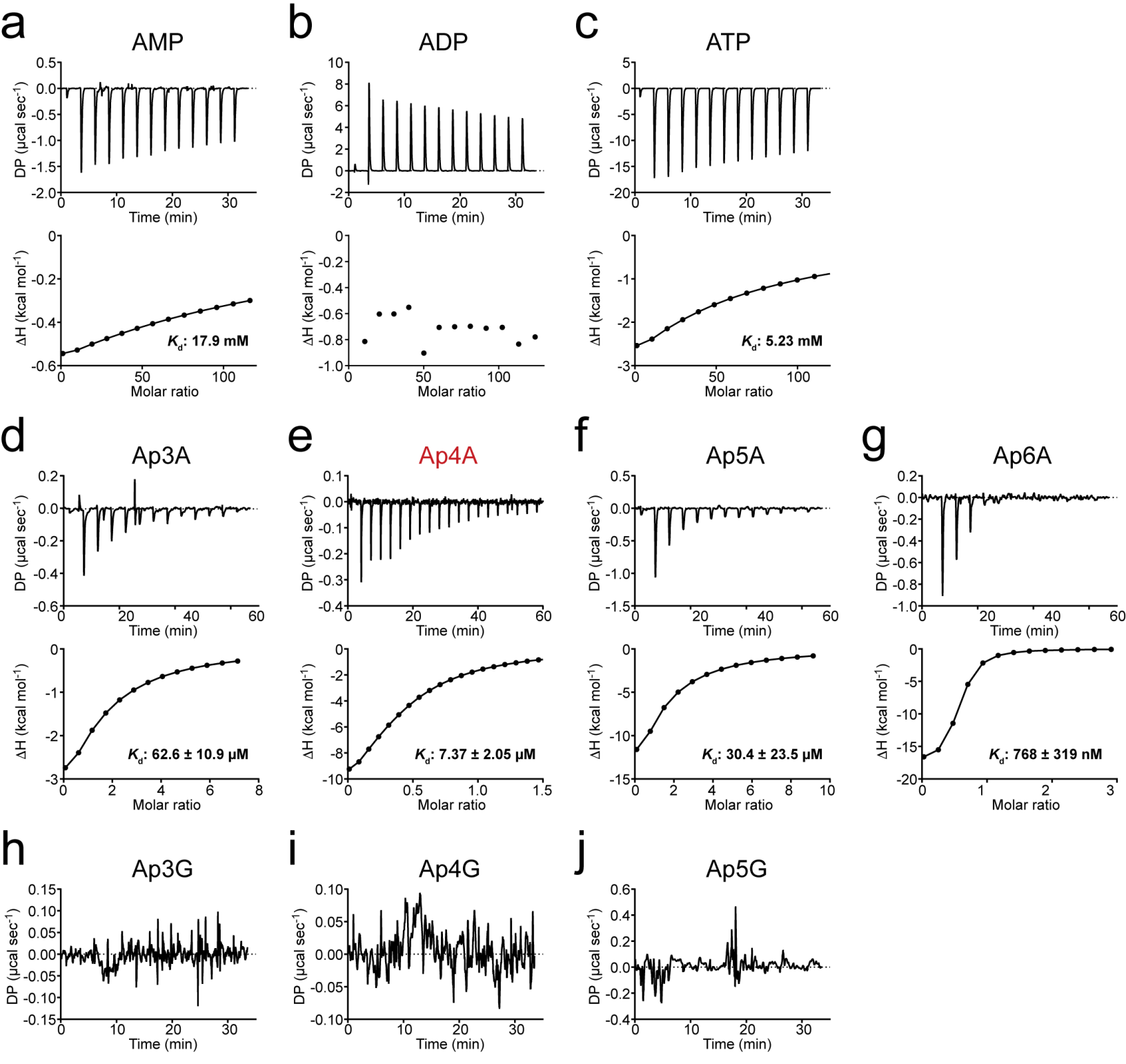
a
AMP
DP (µcal sec⁻¹)
Time (min)
ΔH (kcal mol⁻¹)
$K_d$: 17.9 mM
Molar ratio
b
ADP
DP (µcal sec⁻¹)
Time (min)
ΔH (kcal mol⁻¹)
Molar ratio
c
ATP
DP (µcal sec⁻¹)
Time (min)
ΔH (kcal mol⁻¹)
$K_d$: 5.23 mM
Molar ratio
d
Ap3A
DP (µcal sec⁻¹)
Time (min)
ΔH (kcal mol⁻¹)
$K_d$: 62.6 ± 10.9 µM
Molar ratio
e
Ap4A
DP (µcal sec⁻¹)
Time (min)
ΔH (kcal mol⁻¹)
$K_d$: 7.37 ± 2.05 µM
Molar ratio
f
Ap5A
DP (µcal sec⁻¹)
Time (min)
ΔH (kcal mol⁻¹)
$K_d$: 30.4 ± 23.5 µM
Molar ratio
g
Ap6A
DP (µcal sec⁻¹)
Time (min)
ΔH (kcal mol⁻¹)
$K_d$: 768 ± 319 nM
Molar ratio
h
Ap3G
DP (µcal sec⁻¹)
Time (min)
i
Ap4G
DP (µcal sec⁻¹)
Time (min)
j
Ap5G
DP (µcal sec⁻¹)
Time (min)

a

| | $V_{max}$ (µM min$^{-1}$) | $K_m$ (µM) | $K_i$ (µM) |
|---|---|---|---|
| **No ligand** | 6.3 ± 0.2 | 63.2 ± 9.1 | n.d. |
| **Ap4A 1 µM** | 5.2 ± 0.2 | 58.3 ± 10.7 | |
| **Ap4A 3 µM** | 4.9 ± 0.2 | 47.0 ± 7.2 | |
| **Ap4A 10 µM** | 2.5 ± 0.2 | 41.4 ± 10.5 | 15.8 ± 1.8 |
| **Ap4A 30 µM** | 2.2 ± 0.2 | 35.0 ± 12.5 | |
| **Ap4A 100 µM** | 1.8 ± 0.1 | 41.0 ± 7.5 | |
| **AMP 2 mM** | 5.3 ± 0.2 | 71.2 ± 6.9 | n.d. |
| **ADP 2 mM** | 4.2 ± 0.2 | 62.4 ± 11.2 | n.d. |
| **ATP 2 mM** | 5.1 ± 0.2 | 94.7 ± 13.9 | n.d. |
| **Ap3A 10 µM** | 5.6 ± 0.3 | 58.8 ± 12.4 | n.d. |
| **Ap5A 10 µM** | 2.4 ± 0.2 | 23.7 ± 13.2 | n.d. |
| **Ap6A 10 µM** | 4.9 ± 0.1 | 46.5 ± 4.3 | n.d. |
| **Ap3G 10 µM** | 6.6 ± 0.2 | 47.5 ± 4.6 | n.d. |
| **Ap4G 10 µM** | 6.5 ± 0.2 | 71.9 ± 7.6 | n.d. |
| **Ap5G 10 µM** | 5.9 ± 0.3 | 59.6 ± 13.3 | n.d. |

b

| | $V_{max}$ (µM min$^{-1}$) | $K_m$ (µM) | $K_i$ (µM) |
|---|---|---|---|
| **No ligand** | 8.1 ± 0.3 | 773 ± 81 | n.a. |
| **Ap4A 1 µM** | 5.9 ± 0.2 | 746 ± 77 | |
| **Ap4A 3 µM** | 5.9 ± 0.2 | 858 ± 82 | |
| **Ap4A 10 µM** | 4.2 ± 0.1 | 881 ± 66 | 25.7 ± 2.9 |
| **Ap4A 30 µM** | 3.3 ± 0.2 | 636 ± 73 | |
| **Ap4A 100 µM** | 2.0 ± 0.2 | 346 ± 97 | |

c

| | **No ligand** | | **100 µM Ap4A** | | **2 mM ATP** | |
|---|---|---|---|---|---|---|
| ***Bs*IMPDH** | $V_{max}$ (µM min$^{-1}$) | $K_m$ (µM) | $V_{max}$ (µM min$^{-1}$) | $K_m$ (µM) | $V_{max}$ (µM min$^{-1}$) | $K_m$ (µM) |
| **WT** | 6.3 ± 0.2 | 63.2 ± 9.1 | 1.8 ± 0.1 | 41.0 ± 7.5 | 5.1 ± 0.2 | 94.7 ± 13.9 |
| **K202A** | 9.3 ± 0.3 | 27.8 ± 4.3 | 6.5 ± 0.2 | 35.6 ± 4.4 | 9.2 ± 0.2 | 32.4 ± 2.7 |
| **R141A/R144A** | 12.3 ± 0.2 | 25.2 ± 2.4 | 11.5 ± 0.3 | 31.4 ± 3.8 | 12.4 ± 0.3 | 30.2 ± 3.2 |
| **ΔCBS** | 10.6 ± 0.4 | 14.2 ± 4.5 | 11.7 ± 0.4 | 32.2 ± 5.4 | 11.3 ± 0.2 | 45.8 ± 4.4 |

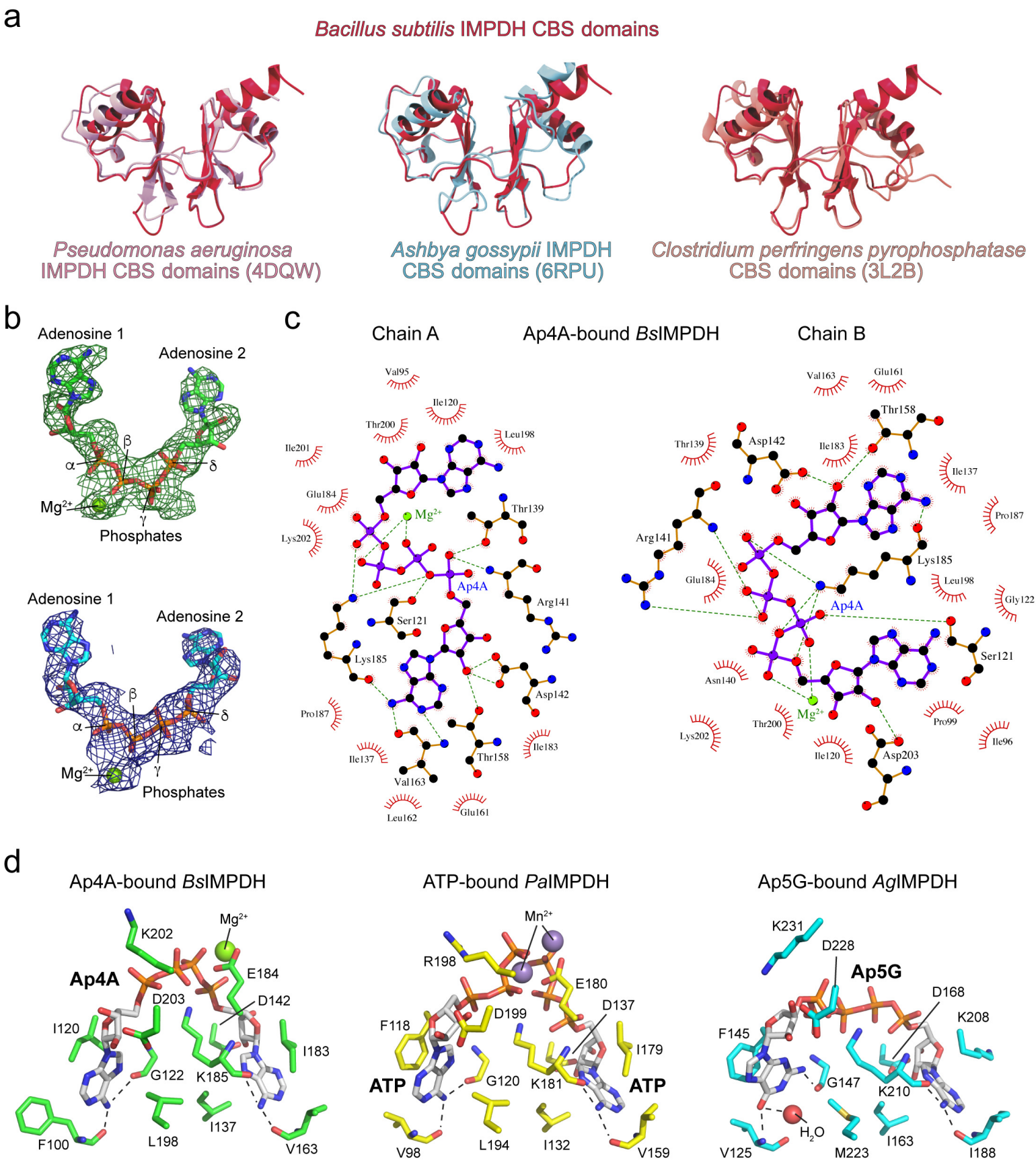
a
Bacillus subtilis IMPDH CBS domains
Pseudomonas aeruginosa IMPDH CBS domains (4DQW)
Ashbya gossypii IMPDH CBS domains (6RPU)
Clostridium perfringens pyrophosphatase CBS domains (3L2B)
b
Adenosine 1
Adenosine 2
Mg2+
Phosphates
c
Chain A
Ap4A-bound BsIMPDH
Chain B
Ap4A
d
Ap4A-bound BsIMPDH
ATP-bound PaIMPDH
Ap5G-bound AgIMPDH
Ap5G
ATP
H2O

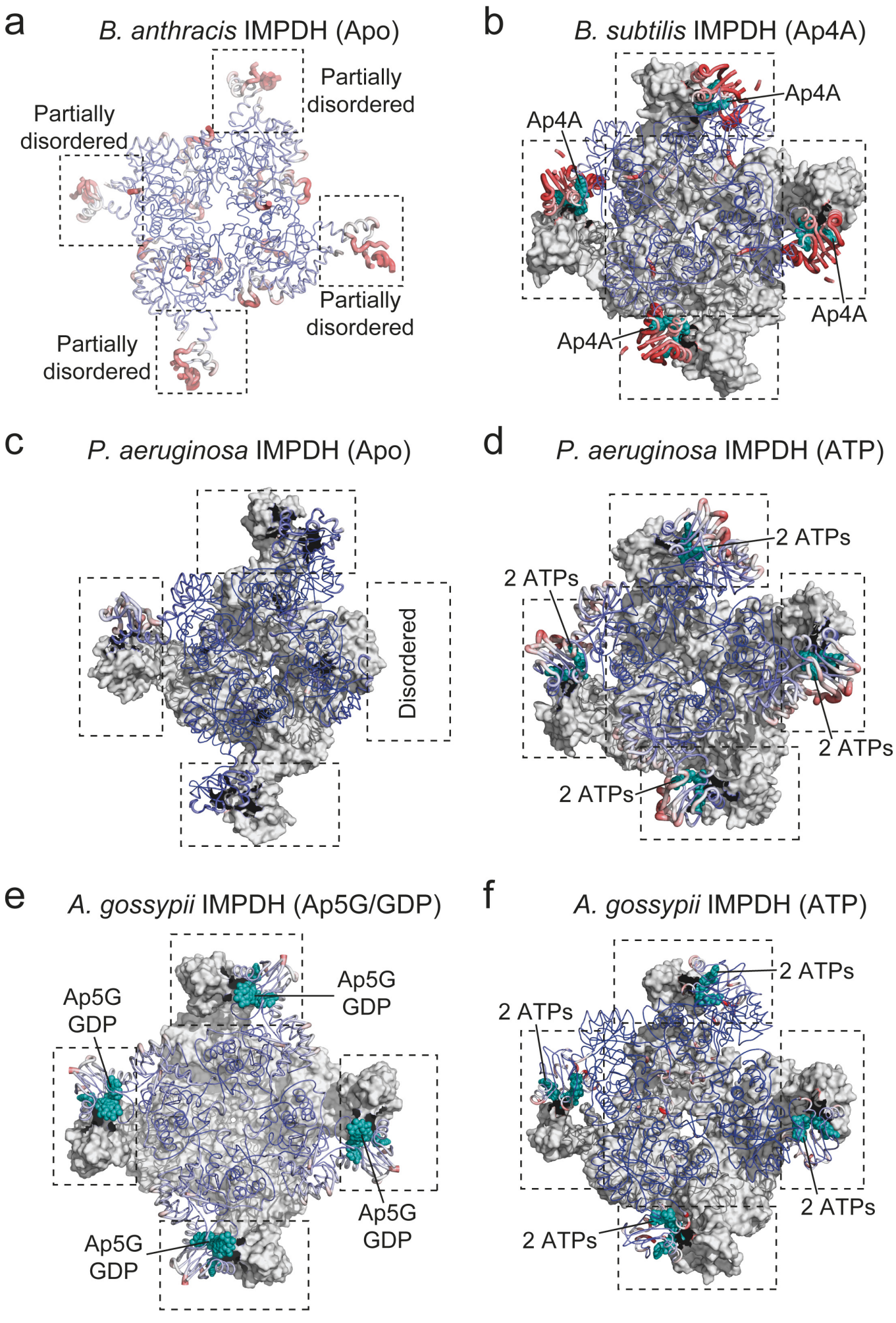
a
B. anthracis IMPDH (Apo)
Partially disordered
Partially disordered
Partially disordered
Partially disordered
Partially disordered
b
B. subtilis IMPDH (Ap4A)
Ap4A
Ap4A
Ap4A
Ap4A
c
P. aeruginosa IMPDH (Apo)
Disordered
d
P. aeruginosa IMPDH (ATP)
2 ATPs
2 ATPs
2 ATPs
2 ATPs
e
A. gossypii IMPDH (Ap5G/GDP)
Ap5G GDP
Ap5G GDP
Ap5G GDP
Ap5G GDP
f
A. gossypii IMPDH (ATP)
2 ATPs
2 ATPs
2 ATPs
2 ATPs

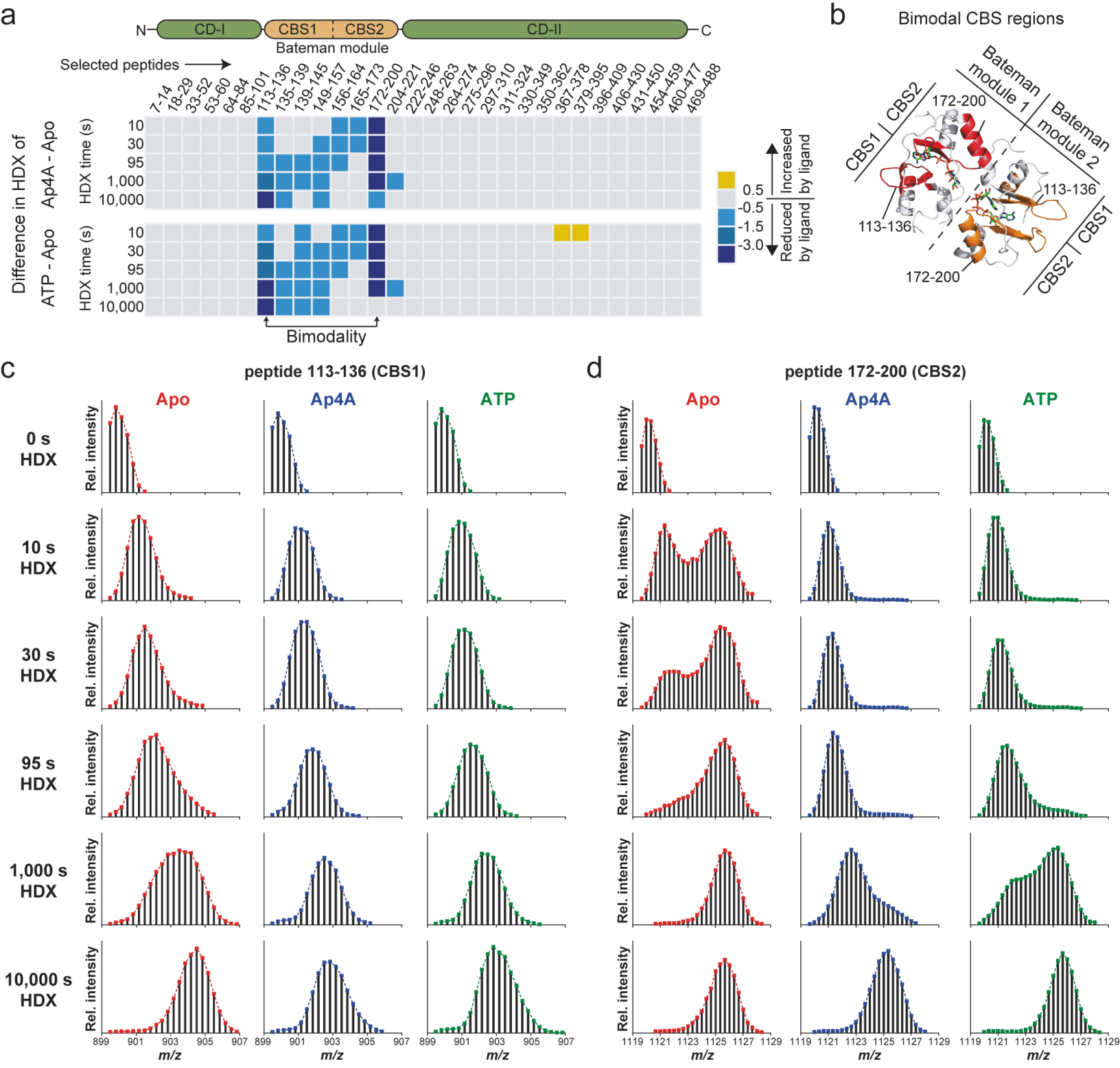
a
N
CD-I
CBS1
CBS2
CD-II
C
Bateman module
Selected peptides
7-14
18-29
33-52
53-60
64-84
85-101
113-136
135-139
139-145
149-157
156-164
165-173
172-200
204-221
222-246
248-263
264-274
275-296
297-310
311-324
330-349
350-362
367-378
379-395
396-409
406-430
431-450
454-459
460-477
469-488
Difference in HDX of
Ap4A - Apo
ATP - Apo
HDX time (s)
10
30
95
1,000
10,000
0.5
-0.5
-1.5
-3.0
Increased by ligand
Reduced by ligand
Bimodality
b
Bimodal CBS regions
Bateman module 1
Bateman module 2
CBS1
CBS2
172-200
113-136
c
peptide 113-136 (CBS1)
d
peptide 172-200 (CBS2)
Apo
Ap4A
ATP
0 s HDX
10 s HDX
30 s HDX
95 s HDX
1,000 s HDX
10,000 s HDX
Rel. intensity
m/z

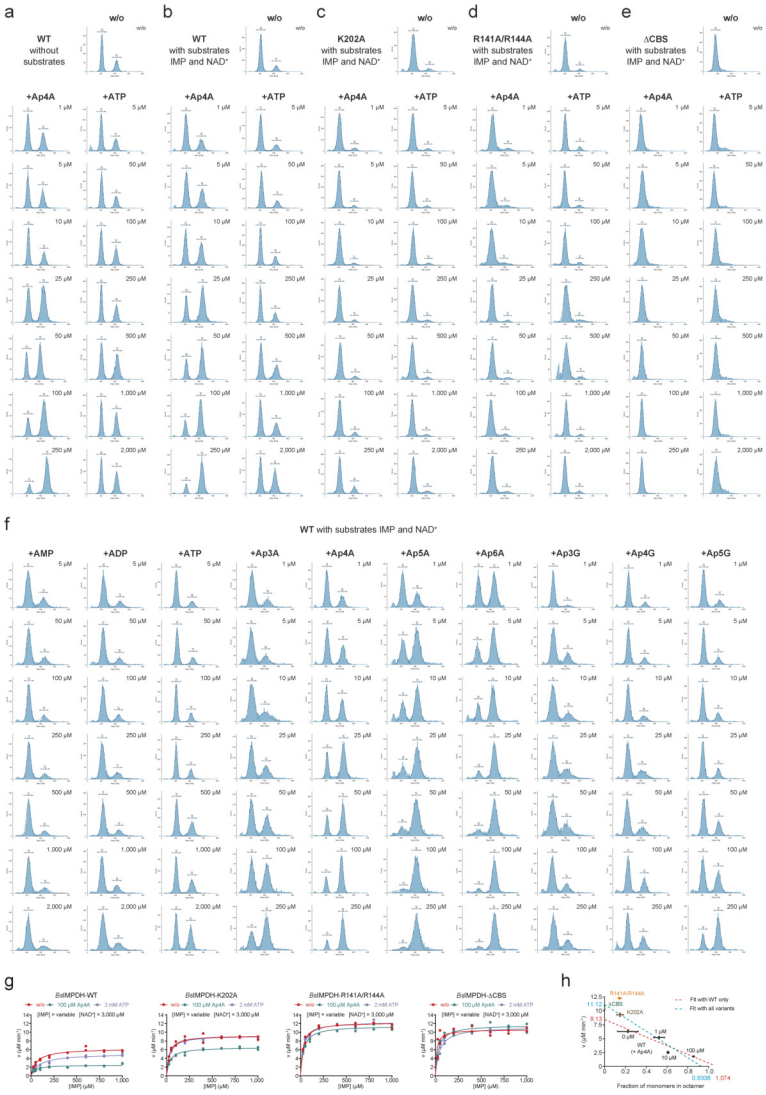
a
WT
without
substrates
w/o
+Ap4A
+ATP
b
WT
with substrates
IMP and NAD+
c
K202A
with substrates
IMP and NAD+
d
R141A/R144A
with substrates
IMP and NAD+
e
ΔCBS
with substrates
IMP and NAD+
f
WT with substrates IMP and NAD+
+AMP
+ADP
+ATP
+Ap3A
+Ap4A
+Ap5A
+Ap6A
+Ap3G
+Ap4G
+Ap5G
g
BstIMPDH-WT
BstIMPDH-K202A
BstIMPDH-R141A/R144A
BstIMPDH-ΔCBS
w/o
100 µM Ap4A
2 mM ATP
[IMP] = variable, [NAD+] = 3,000 µM
v (µM min-1)
[IMP] (µM)
h
R141A/R144A
ΔCBS
K202A
WT
(+ Ap4A)
0 µM
1 µM
10 µM
100 µM
Fit with WT only
Fit with all variants
0.9338
1.074
Fraction of monomers in octamer

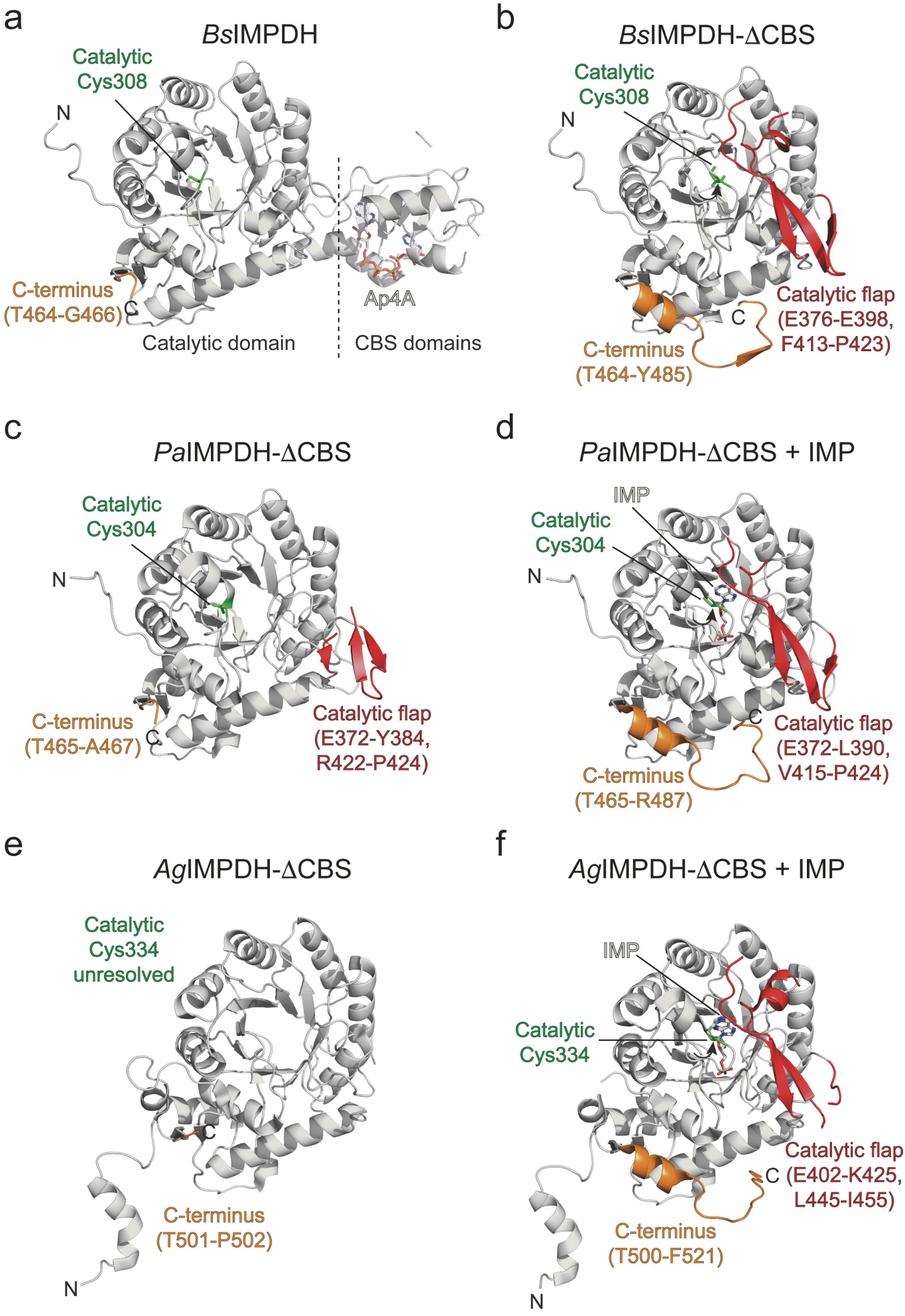
a
BsIMPDH
Catalytic
Cys308
N
C-terminus
(T464-G466)
C
Ap4A
Catalytic domain
CBS domains
b
BsIMPDH-ΔCBS
Catalytic
Cys308
N
Catalytic flap
(E376-E398,
F413-P423)
C
C-terminus
(T464-Y485)
c
PaIMPDH-ΔCBS
Catalytic
Cys304
N
C-terminus
(T465-A467)
C
Catalytic flap
(E372-Y384,
R422-P424)
d
PaIMPDH-ΔCBS + IMP
IMP
Catalytic
Cys304
N
C
Catalytic flap
(E372-L390,
V415-P424)
C-terminus
(T465-R487)
e
AgIMPDH-ΔCBS
Catalytic
Cys334
unresolved
C
C-terminus
(T501-P502)
N
f
AgIMPDH-ΔCBS + IMP
IMP
Catalytic
Cys334
Catalytic flap
C (E402-K425,
L445-I455)
C-terminus
(T500-F521)
N

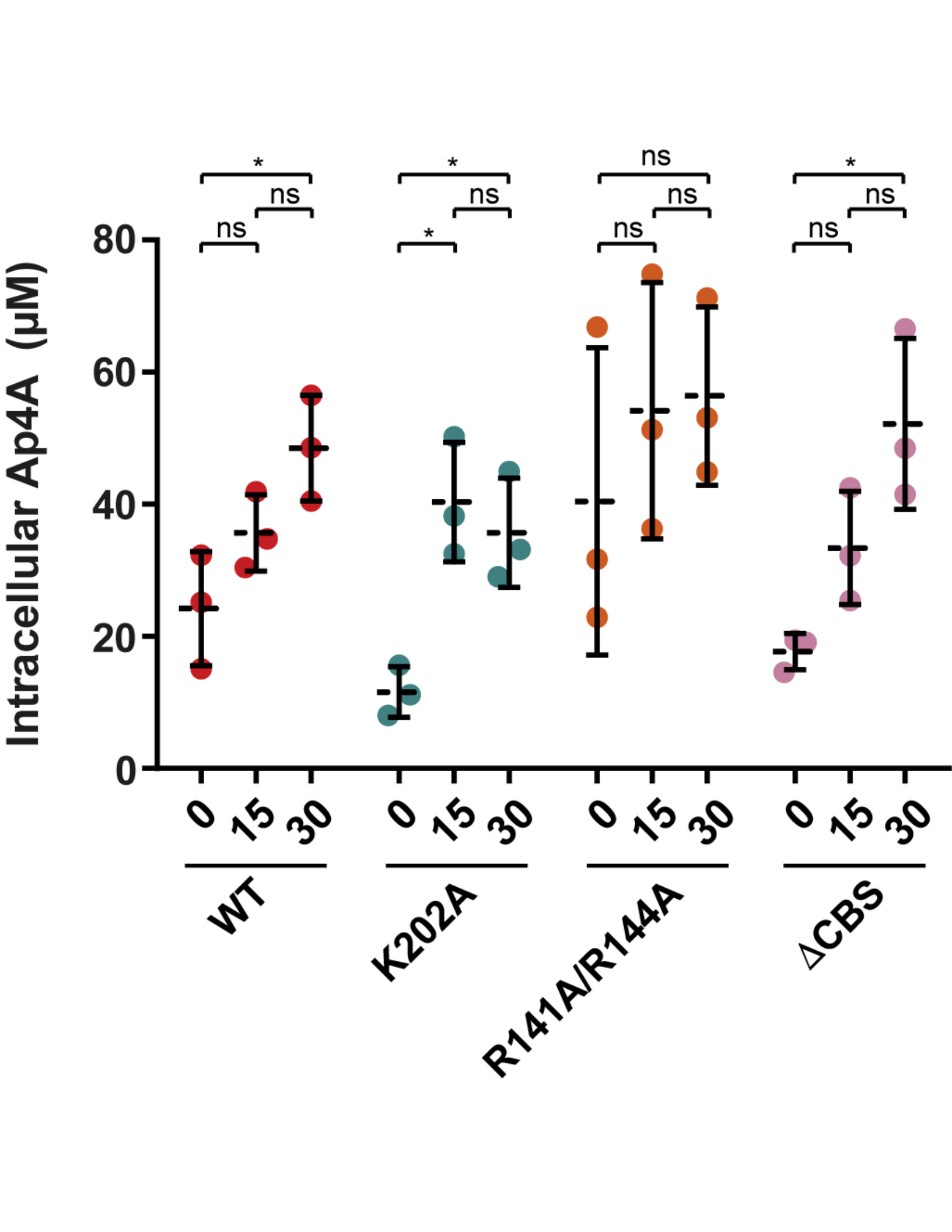
Intracellular Ap4A (μM)
80
60
40
20
0
*
ns
ns
*
*
ns
ns
*
ns
ns
ns
*
ns
ns
0
15
30
0
15
30
0
15
30
0
15
30
WT
K202A
R141A/R144A
ΔCBS